A Comparative Study of π-Arene-Bridged Lanthanum Arylamide and Aryloxide Dimers. Solution Behavior, Exchange Mechanisms, and X-ray Crystal Structures of La$_2$(NH-2,6-^{i}Pr$_2$C$_6$H$_3$)$_6$, La(NH-2,6-^{i}Pr$_2$C$_6$H$_3$)$_3$(THF)$_3$, and La(NH-2,6-^{i}Pr$_2$C$_6$H$_3$)$_3$(py)$_2$

Garth R. Giesbrecht,[1a] John C. Gordon,*,[1b] David L. Clark,*,[1c] P. Jeffrey Hay,[1d] Brian L. Scott,[1b] and C. Drew Tait[1b]

Contribution from the Nuclear Materials Technology (NMT) Division, Chemistry (C) Division, the Glenn T. Seaborg Institute for Transactinium Science and Theoretical (T) Division, Los Alamos National Laboratory, Los Alamos, New Mexico 87545

Received November 26, 2003; E-mail: john.gordon@science.doe.gov

Abstract: Reaction of 3 equiv of 2,6-diisopropylaniline with La[N(SiMe$_3$)$_2$]$_3$ produces the dimeric species La$_2$(NHAr)$_6$ (**1**). X-ray crystallography reveals a centrosymmetric structure, where the dimeric unit is bridged by intermolecular η^6-arene interactions of a unique arylamide ligand attached to an adjacent metal center. Exposure of **1** to THF results in formation of the monomeric tris-THF adduct La(NHAr)$_3$(THF)$_3$ (**2**), which was shown by X-ray crystallography to maintain a *fac*-octahedral structure in the solid state. ^{1}H NMR spectroscopy illustrates that the binding of THF to **1** to form **2** is reversible and removal of THF under vacuum regenerates dimeric **1**. Addition of pyridine to **1** yields the monomeric bis-pyridine adduct La(NHAr)$_3$(py)$_2$ (**3**), which exhibits a distorted trigonal-bipyramidal La metal center. Solution ^{1}H NMR, IR, and Raman spectroscopy indicate that the π-arene-bridged dimeric structure of **1** is maintained in solution. Variable-temperature ^{1}H NMR spectroscopic investigations of **1** are consistent with a monomer–dimer equilibrium at elevated temperature. In contrast, variable-temperature ^{1}H NMR spectroscopic investigations of the aryloxide analogue La$_2$(OAr)$_6$ (**4**) show that the bridging and terminal aryloxide groups exchange by a mechanism in which the dimeric nature of the compound is retained. Density functional theory (DFT) calculations were carried out on model compounds La$_2$(OC$_6$H$_5$)$_6$, La$_2$(NHC$_6$H$_5$)$_6$, and (C$_6$H$_5$R)La(XC$_6$H$_5$)$_3$, where X = O or NH and R = H, OH, or NH$_2$. The formation of η^6-arene interactions is energetically favored over monomeric LaX$_3$ (X = OPh or NHPh) with the aryloxide π-arene interaction being stronger than the arylamide π-arene interaction. Calculation of vibrational frequencies reveals the origin of the observed IR spectral behavior of both La$_2$(OC$_6$H$_5$)$_6$ and La$_2$(NHC$_6$H$_5$)$_6$, with the higher energy ν(C=C) stretch due to terminal ligands and the lower energy stretch associated with the bridging ligands.

Introduction

The identification of alternative ligand systems capable of stabilizing monomeric lanthanide species while provoking novel reactivity is a prevalent theme in contemporary 4f-element chemistry.[2–4] To this end, bulky aryloxide anions OAr$^-$ have been extensively investigated as ancillary ligands due to the ability to modify both the electronic and steric properties of the resultant complexes by varying the substituents on the phenyl ring.[5,6] This theory is borne out by the observation of varying structural modes upon changing the size of the group at the 2-

and 6-positions of the phenyl ring: for example, use of the sterically demanding 2,6-di-*tert*-butylphenoxide group leads to the formation of mononuclear Ln(OAr)$_3$ complexes for the entire lanthanide series,[7] whereas the less sterically encumbered 2,6-dimethylphenoxide results in formation of dimeric Lewis base adducts Ln$_2$(O-2,6-Me$_2$C$_6$H$_3$)$_6$L$_4$ (Ln = Y,[8] Nd;[9] L = THF). It has also been shown that f-element complexes containing less sterically demanding aliphatic alkoxide ligands such as neopentoxide[10] or *tert*-butoxide[11–13] show a strong tendency toward oligomerization, resulting in the isolation of trinuclear or higher

(1) (a) NMT-DO, Mail Stop J514. (b) C-SIC, Mail Stop J514. (c) G. T. Seaborg Institute, Mail Stop E500. (d) T-12, Mail Stop B268.
(2) Edelmann, F. T. *Angew. Chem., Int. Ed. Engl.* **1995**, *34*, 2466.
(3) Edelmann, F. T.; Freckmann, D. M. M.; Schumann, H. *Chem. Rev.* **2002**, *102*, 1851.
(4) Piers, W. E.; Emslie, D. J. H. *Coord. Chem. Rev.* **2002**, *233*, 131.
(5) Mehrotra, R. C.; Singh, A.; Tripathi, U. M. *Chem. Rev.* **1991**, *91*, 1287.
(6) Barnhart, D. M.; Clark, D. L.; Gordon, J. C.; Huffman, J. C.; Vincent, R. L.; Watkin, J. G.; Zwick, B. D. *Inorg. Chem.* **1994**, *33*, 3487 and references therein.

(7) Hitchcock, P. B.; Lappert, M. F.; Singh, A. *Chem. Commun.* **1983**, 1499.
(8) Evans, W. J.; Olofson, J. M.; Ziller, J. W. *Inorg. Chem.* **1989**, *28*, 4308.
(9) Evans, W. J.; Ansari, M. A.; Khan, S. I. *Organometallics* **1995**, *14*, 558.
(10) Barnhart, D. M.; Clark, D. L.; Gordon, J. C.; Huffmann, J. C.; Watkin, J. G.; Zwick, B. D. *J. Am. Chem. Soc.* **1993**, *115*, 8461.
(11) Bradley, D. C.; Chudzynska, H.; Hursthouse, M. B.; Motevalli, M. *Polyhedron* **1991**, *10*, 1049.
(12) Veith, M.; Mathur, S.; Kareiva, A.; Jilavi, M.; Zimmer, M.; Huch, V. *J. Mater. Chem.* **1999**, *9*, 3069.
(13) Gromada, J.; Chenal, T.; Mortreux, A.; Ziller, J. W.; Leising, F.; Carpentier, J. F. *Chem. Commun.* **2000**, 2183.

order oligomers, illustrating the potential degree of control over nuclearity in these systems. The coordination and reaction chemistry of such species has been extensively documented and has been the subject of much discussion.[14,15]

In contrast to the considerable literature available on lanthanide aryloxide (OAr) systems, much less is known about the analogous arylamide (NHAr) derivatives. Although the chemistry of polydentate nitrogen-based systems is an increasingly popular avenue of study,[16,17] the chemistry of lanthanides supported by simple amido ligands is generally dominated by the bistrimethylsilyl derivative N(SiMe₃)₂⁻.[18–21] Considering the ubiquitous presence of aryloxide ligands in lanthanide chemistry,[22,23] it is curious that the corresponding arylamido chemistry is so underdeveloped. Evans and co-workers were the first to report the utility of such ligands with yttrium and the lanthanides,[24] and we and others have since employed the 2,6-diisopropylanilido ligand to advance the chemistry of lanthanide−imido functionalities.[25,26] Despite these reports, little is known about the comparative behavior of aryloxide and arylamide ligands when complexed to the lanthanides. Here we report the synthesis and solution behavior of La₂(NHAr)₆ (Ar = 2,6-^{i}Pr₂C₆H₃), and its complexation with Lewis bases. We compare the observed chemistry of this arylamide system with the structurally related aryloxide La₂(OAr)₆ (Ar = 2,6-^{i}Pr₂C₆H₃)[27] and offer insights into the nature and relative strengths of La−OAr versus La−NHAr bonding.

Results and Discussion

I. Synthesis and Reactivity. Reaction of monomeric La[N(SiMe₃)₂]₃ with 3 equiv of 2,6-diisopropylaniline in refluxing toluene solution produces the bright yellow dimeric complex La₂(NHAr)₆ (**1**) (Ar = 2,6-^{i}Pr₂C₆H₃) in moderate yield (eq 1). Compound **1** is only sparingly soluble in pentane or

$$2La[N(SiMe_3)_2]_3 + 6H_2NAr \xrightarrow[-6HN(SiMe_3)_2]{toluene, \Delta} \underset{\textbf{1}}{La_2(NHAr)_6} \quad (1)$$

$$Ar = 2,6\text{-}^iPr_2C_6H_3$$
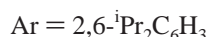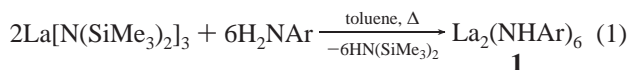
hexane but has increased solubility in aromatic solvents. This is in contrast to the previously reported Y, Yb, and Sm analogues, which were found to be virtually insoluble in noncoordinating solvents.[24,25] The higher solubility of the lanthanum derivative may be attributed to the larger size of the La metal center.[28] The monomeric Lewis base adduct La(NHAr)₃-(THF)₃ (**2**) is conveniently prepared by simple dissolution of

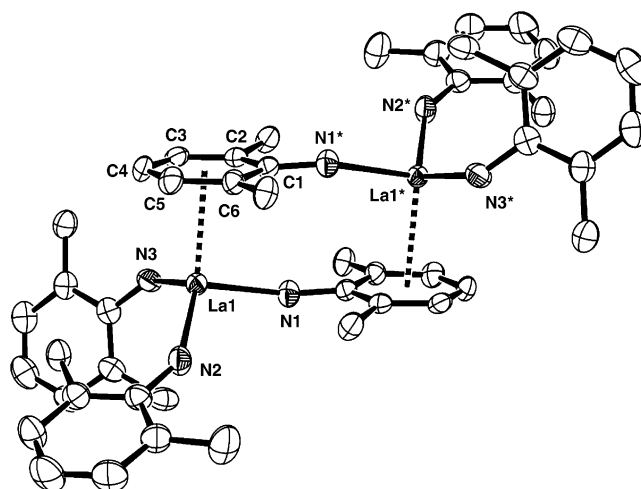(14) van der Sluys, W. G.; Sattelberger, A. P. *Chem. Rev.* **1990**, *90*, 1027.
(15) Barnhart, D. M.; Clark, D. L.; Gordon, J. C.; Huffman, J. C.; Watkin, J. G.; Zwick, B. D. *Inorg. Chem.* **1995**, *34*, 5416 and references therein.
(16) Gade, L. H. *Chem. Commun.* **2000**, 173.
(17) Kempe, R. *Angew. Chem., Int. Ed.* **2000**, *39*, 468.
(18) Alyea, E. C.; Bradley, D. C.; Copperwaite, R. G. *Dalton Trans.* **1972**, 1580.
(19) Bradley, D. C.; Ghotra, J. G.; Hart, F. A. *Dalton Trans.* **1973**, 1021.
(20) Ghotra, J. S.; Hursthouse, M. B.; Welch, A. J. *Chem. Commun.* **1973**, 669.
(21) Evans, W. J.; Golden, R. E.; Ziller, J. W. *Inorg. Chem.* **1991**, *30*, 4963.
(22) Bradley, D. C.; Mehrotra, R. C.; Gaur, D. P. *Metal Alkoxides*; Academic Press: London, 1978.
(23) Chisholm, M. H.; Rothwell, I. P. In *Comprehensive Coordination Chemistry*; Wilkinson, G., Gillard, R., McCleverty, J. A., Eds.; Pergamon Press: London, 1987; Vol. 2.
(24) Evans, W. J.; Ansari, M. A.; Ziller, J. W.; Khan, S. I. *Inorg. Chem.* **1996**, *35*, 5435.
(25) Gordon, J. C.; Giesbrecht, G. R.; Clark, D. L.; Hay, P. J.; Keogh, D. W.; Poli, R.; Scott, B. L.; Watkin, J. G. *Organometallics* **2002**, *21*, 4726.
(26) Chan, H. S.; Li, H. W.; Xie, Z. *Chem. Commun.* **2002**, 652.
(27) Butcher, R. J.; Clark, D. L.; Grumbine, S. K.; Vincent-Hollis, R. L.; Scott, B. L.; Watkin, J. G. *Inorg. Chem.* **1995**, *34*, 5468.
(28) Shannon, R. D. *Acta Crystallogr., Sect. A* **1976**, *32*, 751.

Figure 1. Thermal ellipsoid view of La₂(NH-2,6-^{i}Pr₂C₆H₃)₆ (**1**) drawn with 30% probability ellipsoids and emphasizing the η^6-arene and the local three-legged piano stool geometry about the La metal center. Isopropyl methyl groups have been omitted for clarity.

La₂(NHAr)₆ (**1**) in THF. Slow evaporation of the solvent yields **2** as large colorless crystals in good yield (eq 2). Compound **2**

$$La_2(NHAr)_6 \underset{-THF}{\overset{+THF}{\rightleftharpoons}} \underset{\textbf{2}}{La(NHAr)_3(THF)_3} \quad (2)$$
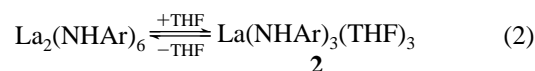
has increased solubility compared to that of the unsolvated dimer **1**, readily dissolving in aromatic solvents such as benzene or toluene as well as in coordinating solvents such as THF. The reaction outlined in eq 2 is found to be chemically reversible. Removal of THF under dynamic vacuum over a toluene solution regenerates dimeric **1** in near quantitative yield. Addition of pyridine to a toluene solution of **1** yields the monomeric bis-pyridine adduct La(NHAr)₃(py)₂ (**3**) in good yield (eq 3).

$$La_2(NHAr)_6 \xrightarrow[toluene]{xs \ pyridine} \underset{\textbf{3}}{2La(NHAr)_3(py)_2} \quad (3)$$
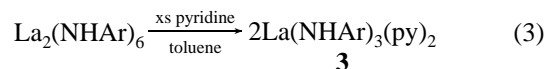
Compound **3** is isolated as a bright yellow solid with similar solubility characteristics to those of the tris-THF adduct **2**. The formation of the pyridine adduct **3** is not chemically reversible. Compounds **1**−**3** are moisture sensitive but are indefinitely stable when stored under an inert atmosphere, showing no signs of decomposition after months at ambient temperature.

II. Solid-State and Molecular Structures. A. La₂(NH-2,6-^{i}Pr₂C₆H₃)₆ (1). Slow evaporation of a saturated toluene solution of **1** yielded yellow crystalline blocks that were suitable for X-ray diffraction. The solid-state molecular structure of **1** is presented in Figure 1. A listing of relevant bond lengths and angles is available in Table 1; complete details of the structural analyses of compounds **1**−**3** are listed in Table 4. Compound **1** possesses a centrosymmetric π-arene-bridged dimeric structure analogous to that reported for the Y and Sm analogues,[24,25] as well as the f-element diisopropylphenoxide dimers M₂(OAr)₆ (M = La, Nd, Sm, U).[6,27,29] In the solid-state structure of **1**, each La atom is ligated by three N atoms of arylamido ligands, and each metal center engages in an η^6-arene interaction with the aryl ring of an arylamido ligand attached to an adjacent La center. The three N atoms and the aryl ring centroid support a

(29) van der Sluys, W. G.; Burns, C. J.; Huffman, J. C.; Sattelberger, A. P. *J. Am. Chem. Soc.* **1988**, *110*, 5924.

***Table 1.*** Selected Bond Distances^a (Å) and Angles (deg) for La$_2$(NH-2,6-^{i}Pr$_2$C$_6$H$_3$)$_6$ (**1**)

La1−N1	2.434(3)	La1−N2	2.347(4)
La1−N3	2.360(3)	La1−arene(cent)	2.730
La1−C1	3.209(4)	La1−C2	3.129(4)
La1−C3	3.028(3)	La1−C4	2.972(3)
La1−C5	2.995(4)	La1−C6	3.080(4)
N1−La1−N2	111.27(11)	N1−La1−N3	93.12(11)
N1−La1−arene(cent)	98.47	N2−La1−N3	122.37(12)
N2−La1−arene(cent)	122.11	N3−La1−arene(cent)	103.32
La1−N1−C1	151.0(3)	La1−N2−C13	149.3(2)
La1−N3−C25	136.4(3)		

^{a} cent = centroid of C$_6$H$_5$.

pseudo-tetrahedral geometry around the central metal atom, with the angles anchored by the La atom ranging from 93.12(11)° to 122.37(12)°. The coordination geometry of each La atom approximates that of a three-legged piano stool. The distances between the La metal center and the six C atoms of the arene ring range from 2.972(3) to 3.209(4) Å with an average distance of 3.069(4) Å (La(1)−arene(cent) = 2.730 Å). This average La−C bond distance is similar to those reported for the structurally related aryloxide species La$_2$(O-2,6-^{i}Pr$_2$C$_6$H$_3$)$_6$ (La−C ave = 3.062(10) Å; range = 2.978(10)−3.164(9) Å)[27] and are somewhat longer than the Sm−C$_{arene}$ bonds found in the Sm analogue Sm$_2$(NHAr)$_6$ (Sm−C ave = 2.952(10) Å; range = 2.838(10)−3.094(10) Å),[25] in accord with the larger ionic radius of La. The La−N distances for terminal arylamido ligands in **1** (2.347(4) and 2.360(3) Å) are slightly shorter than the bridging La−N distance (2.434(3) Å) and are in the expected range reported for other lanthanum−amido bonds. Again, the La−N bond lengths are slightly longer than those observed in Sm$_2$(NHAr)$_6$. The La−N−C bond angle for the bridging ligand is 151.0(3)° and the La−N−C bond angles for the terminal ligands are 136.4(3)° and 149.3(2)°.

B. La(NH-2,6-^{i}Pr$_2$C$_6$H$_3$)$_3$(THF)$_3$ (2). Slow evaporation of a saturated THF solution of **2** yielded large colorless blocks that were amenable to X-ray diffraction. The molecular structure of **2** is shown in Figure 2, with selected bond lengths and angles given in Table 2. The complex crystallizes as discrete molecules with no unusual intermolecular contacts. The three arylamido ligands and the three THF molecules in **2** define a distorted octahedron with the NHAr groups arranged in a facial geometry about the La center. The angles involving the arylamido ligands are all larger than 90° (N1−La1−N2 = 107.7(2)°, N1−La1−N3 = 107.9(2)°, N2−La1−N3 = 119.9(2)°) whereas those involving THF groups are all smaller than 90° (O1−La1−O2 = 77.8(1)°, O1−La1−O3 = 77.9(1)°, O2−La1−O3 = 74.2-(1)°), reflecting the steric demands of the diisopropylanilido groups. The overall geometric features are similar to those determined for the Nd analogue Nd(NH-2,6-^{i}Pr$_2$C$_6$H$_3$)$_3$(THF)$_3$[24] and the aryloxide complex Y(O-2,6-Me$_2$C$_6$H$_3$)$_3$(THF)$_3$.[8] In contrast, the La diisopropylphenoxide compound La(O-2,6-^{i}Pr$_2$C$_6$H$_3$)$_3$(THF)$_2$ crystallizes as a bis-THF adduct, resulting in a trigonal bipyramidal metal center.[27] The La−N distances in **2** (2.379(6) − 2.401(5) Å) are slightly longer than the La−O distances reported for La(OC$_6$H$_3$^{i}Pr$_2$-2,6)$_3$(THF)$_2$ (2.169(7) − 2.233(8) Å), resulting in a less crowded coordination sphere, allowing for the presence of an additional THF ligand. The La−N distances are also longer than the analogous metal-arylamido distances in Nd(NH-2,6-^{i}Pr$_2$C$_6$H$_3$)$_3$(THF)$_3$ (2.304(8) − 2.320(8) Å) as a result of the larger ionic radius of La versus
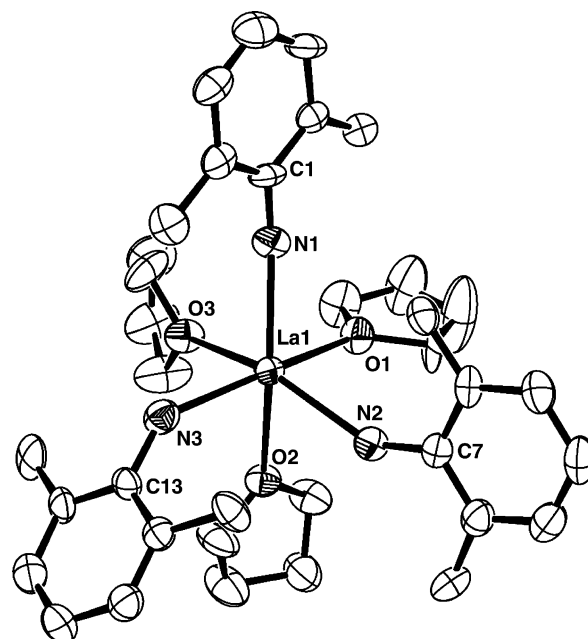
Figure 2. Thermal ellipsoid view of La(NH-2,6-^{i}Pr$_2$C$_6$H$_3$)$_3$(THF)$_3$ (**2**) drawn with 30% probability ellipsoids and illustrating the facial arrangement of NHAr and THF ligands. Isopropyl methyl groups have been omitted for clarity.

Table 2. Selected Bond Distances (Å) and Angles (deg) for La(NH-2,6-^{i}Pr$_2$C$_6$H$_3$)$_3$(THF)$_3$ (**2**)

La1−N1	2.379(6)	La1−N2	2.401(5)
La1−N3	2.395(4)	La1−O1	2.688(4)
La1−O2	2.656(3)	La1−O3	2.671(4)
N1−La1−N2	107.7(2)	N1−La1−N3	107.9(2)
N1−La1−O1	160.0(2)	N1−La1−O2	87.1(2)
N1−La1−O3	85.6(2)	N2−La1−N3	119.9(2)
N2−La1−O1	81.6(2)	N2−La1−O2	76.7(1)
N2−La1−O3	147.3(1)	N3−La1−O1	81.0(2)
N3−La1−O2	150.7(2)	N3−La1−O3	81.8(2)
O1−La1−O2	77.8(1)	O1−La1−O3	77.9(1)
O2−La1−O3	74.2(1)	La1−N1−C1	143.1(4)
La1−N2−C7	149.4(4)	La1−N3−C13	158.6(6)

Nd. The La−O(THF) distances (2.672(3) Å ave) are significantly longer than those observed in La(O-2,6-^{i}Pr$_2$C$_6$H$_3$)$_3$(THF)$_2$ (2.52(1) Å ave) as well as other THF adducts of La such as La(η^5-C$_5$Me$_5$)[CH(SiMe$_3$)$_2$]$_2$(THF) (2.547(6) Å),[30] La(η^5-C$_5$H$_5$)$_3$-(THF) (2.57(1) Å),[31] (η^5:η^1:η^1-C$_5$H$_3$(CH$_2$CH$_2$NMe$_2$)$_2$-1,2)LaI$_2$-(THF) (2.558(3) Å) and (η^5:η^1:η^1-C$_5$H$_3$(CH$_2$CH$_2$NMe$_2$)$_2$-1,3)-LaI$_2$(THF) (2.593(3) Å),[32] although the axial THF La−O(THF) bond length found in La(O-2,6-Ph$_2$C$_6$H$_3$)$_3$(THF)$_2$ is similar to that reported here (2.67(2) Å).[33]

C. La(NH-2,6-^{i}Pr$_2$C$_6$H$_3$)$_3$(py)$_2$ (3). Cooling a saturated toluene solution of **3** to −30 °C yielded the bis-pyridine adduct as large yellow plates. The molecular structure of **3** is presented in Figure 3 with selected bond lengths and angles given in Table 3. Complex **3** maintains a similar geometry to that previously reported for Ln(OAr)$_3$(THF)$_2$ (Ln = La, Pr, Gd, Er, Lu; Ar = 2,6-^{i}Pr$_2$C$_6$H$_3$)[6,27] and consists of a distorted trigonal-bipyramidal

(30) van der Heijden, H.; Schaverien, C. J.; Orpen, A. G. *Organometallics* **1989**, *8*, 255.
(31) Rogers, R. D.; Atwood, J. L.; Emad, A.; Skidora, D. J.; Rausch, M. D. *J. Organomet. Chem.* **1981**, *216*, 383.
(32) Fedushkin, I. L.; Dechert, S.; Schumann, H. *Organometallics* **2000**, *19*, 4066.
(33) Deacon, G. B.; Feng, T.; Skelton, B. W.; White, A. H. *Aust. J. Chem.* **1995**, *48*, 741.
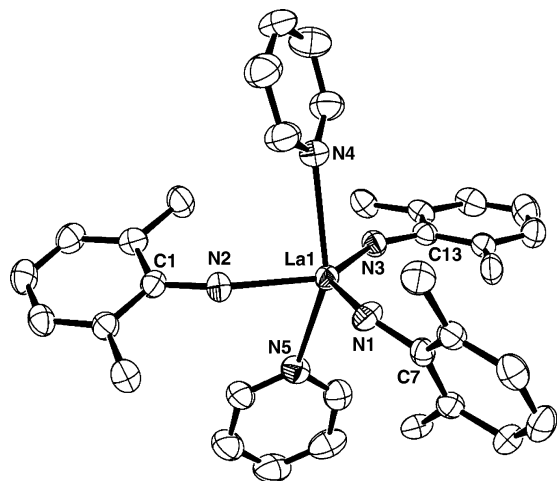
Figure 3. Thermal ellipsoid view of La(NH-2,6-^{i}Pr$_2$C$_6$H$_3$)$_3$(py)$_2$ (**3**) drawn with 30% probability ellipsoids and illustrating the trigonal-bipyramidal coordination between two trans py and three equatorial NHAr ligands. Isopropyl methyl groups have been omitted for clarity.

Table 3. Selected Bond Distances (Å) and Angles (deg) for La(NH-2,6-^{i}Pr$_2$C$_6$H$_3$)$_3$(py)$_2$ (**3**)

La1–N1	2.370(4)	La1–N2	2.354(3)
La1–N3	2.397(4)	La1–N4	2.707(3)
La1–N5	2.729(3)		
N1–La1–N2	91.87(13)	N1–La1–N3	133.58(12)
N1–La1–N4	94.35(12)	N1–La1–N5	112.94(11)
N2–La1–N3	134.53(13)	N2–La1–N4	83.63(10)
N2–La1–N5	83.83(11)	N3–La1–N4	90.32(11)
N3–La1–N5	79.58(11)	N4–La1–N5	150.23(11)
La1–N1–C1	143.8(3)	La1–N2–C7	151.7(3)
La1–N3–C13	149.8(3)		

Table 4. Crystallographic Data^a

	1	2	3
formula	C$_{72}$H$_{108}$N$_6$La$_2$	C$_{52}$H$_{86}$LaN$_3$O$_4$	C$_{46}$H$_{64}$LaN$_5$
mol wt	1335.46	956.15	825.93
temp, K	203(2)	203(2)	203(2)
crystal system	monoclinic	monoclinic	monoclinic
space group	$P2_1/n$	$P2_1$	$P2_1$
crystal size, mm	0.25 × 0.21 × 0.12	0.30 × 0.20 × 0.14	0.29 × 0.21 × 0.12
a, Å	14.066(3)	13.137(4)	16.013(6)
b, Å	15.480(3)	16.922(4)	14.159(5)
c, Å	16.147(3)	13.442(3)	21.202(6)
β, deg	92.652(4)	119.253(3)	112.122(11)
V, Å^3	3512.2(11)	2607.3(11)	4453(3)
Z	4	2	4
D_{calc}, g/cm^3	1.263	1.218	1.232
abs coeff, mm^{-1}	1.242	0.862	0.994
F(000)	1392	1016	1728
θ range, deg	1.8–25.4	1.74–25.36	1.04–25.52
total reflcns	22592	16872	28486
indep reflcns	6185	9402	14478
GOF	1.223	1.274	1.164
R1	0.0452	0.0480	0.0279
wR2	0.0758	0.0956	0.0719

^{a} $R_1 = \Sigma||F_o|-|F_c||/\Sigma|F_o|$ and $R_{2w} = [\Sigma[\omega(F_o{}^2 - F_c{}^2)^2]/\Sigma[\omega(F_o{}^2)^2]]^{1/2}$; $\omega = 1/[\sigma^2(F_o{}^2) + (aP)^2]$, where $a = 0.0326$, 0.0419, and 0.0454.

metal center with three equatorial arylamide ligands and two axial py ligands. A feature common to **3** as well as Ln(O-2,6-^{i}Pr$_2$C$_6$H$_3$)$_3$(THF)$_2$ species is that two arylamido ligands lie with their phenyl rings almost in the plane of the trigonal bipyramid, while the remaining group (containing N1) is twisted, such that the aryl ring is almost perpendicular to the plane. The average

La–N distance to arylamide ligands is 2.374(3) Å and well within the range observed in **1** and **2**. The axial pyridine ligands bend away from this unique arylamido ligand, resulting in an axial N–La–N angle of 150.23(11)°, which is significantly smaller than the expected 180° for a trigonal-bipyramidal molecule. A slight distortion also exists between the arylamido ligands in the equatorial plane, with one smaller N–La–N angle (N1–La1–N2 = 91.87(13)°) and two larger N–La–N angles (N1–La1–N3 = 133.58(12)°; N2–La1–N3 = 134.53(13)°). The La–N$_{arylamido}$–C$_{ipso}$ bond angles are all approximately 150° and similar to those reported for the tris-THF adduct **2**. The bonds between the La atom and the N atoms of the two pyridines are longer than those to the arylamido ligands (La1–N4 = 2.707(3) Å; La1–N5 = 2.729(3) Å). A comparison to other similar compounds is unavailable as solid-state structures of species of the general type Ln(XAr)$_3$(py)$_x$ (Ln = lanthanide; X = O, NH; x = 2, 3) have not been reported; however, the related thorium aryloxide complex Th(O-2,6-Me$_2$C$_6$H$_3$)$_4$(py)$_2$ exhibits Th–N distances of 2.662(8) and 2.696(8) Å.[34]

III. Spectroscopic Characterization. A. Vibrational Spectroscopy. Infrared (IR) spectroscopy has been shown to be diagnostic in the identification of η-arene-bridged dimeric structures for lanthanide and actinide compounds.[6,27] Infrared spectroscopy shows two distinct aromatic ν(C=C) vibrational modes consistent with two different arene environments for π-bound bridging and terminal aryloxide ligands in M$_2$(OAr)$_6$ compounds both in solution and in the solid state. For example, the IR spectra of Ln$_2$(μ-η^6-OAr)$_2$(OAr)$_4$ (Ln = Sm, Nd, Er, and La) reveal a higher frequency band near 1590 cm^{-1} in Nujol and at 1588 cm^{-1} in benzene solution. The second band appears at 1572 cm^{-1} in both the solid state and in solution. The higher energy band is twice the intensity of the lower energy band and corresponds to the terminal aryloxide ligands. The lower energy frequency indicates a weakening of the C=C bond and is consistent with a π-arene bridging interaction. This lower energy feature is absent in all monomeric Lewis base adducts (Table 5). Similar frequencies were also identified for η^6-arene coordination of Ln(SAr*)$_2$ (Ln = Eu, Yb; Ar* = 2,6-Trip$_2$C$_6$H$_3$; Trip = 2,4,6-^{i}Pr$_3$C$_6$H$_2$).[35]

In the present study we employ both IR and Raman spectroscopy and therefore report the Raman of the aryloxide analogue for comparison purposes. The solid-state (Nujol) vibrational spectra of La$_2$(NH-2,6-^{i}Pr$_2$C$_6$H$_3$)$_6$ (**1**) exhibit two distinct ν(C=C) stretching modes in the aromatic region at 1587 and 1575 cm^{-1} in the IR and 1589 and 1576 cm^{-1} in the Raman. This is consistent with maintenance of two different arene environments in solid state, as expected on the basis of the solid-state molecular structure. These two sets of vibrational modes are also evident in both the IR and Raman spectra of La$_2$(O-2,6-^{i}Pr$_2$C$_6$H$_3$)$_6$ (**4**) (Figure 4), with Nujol IR frequencies at 1588 and 1571 cm^{-1} and with the corresponding Raman frequencies at 1591 and 1572 cm^{-1}. This is fully consistent with the presence of the η-arene-bridged dimeric structure observed in the solid state. In comparison, La(NHAr)$_3$(THF)$_3$, with only terminal arylamido ligands, exhibits only one peak in the region at 1588 (IR) and 1589 (Raman) cm^{-1} in the solid state. Vibrational spectra of monomeric La(NHAr)$_3$(py)$_2$ consist of two

(34) Berg, J. M.; Clark, D. L.; Huffman, J. C.; Morris, D. E.; Sattelberger, A. P.; Streib, W. E.; van der Sluys, W. G.; Watkin, J. G. *J. Am. Chem. Soc.* **1992**, *114*, 10811.
(35) Niemeyer, M. *Eur. J. Inorg. Chem.* **2001**, 1969.

Table 5. Infrared Vibrational Frequencies (cm^{-1}) for the ν(C=C) Stretch in 2,6-Diisopropylphenoxide and 2,6-Diisopropylanilide Complexes

compound	ν(C=C)		medium	ref
Arylamides				
La$_2$(NHAr)$_6$	1587	1575	Nujol	this work
La$_2$(NHAr)$_6$	1588	1572	benzene	this work
Sm$_2$(NHAr)$_6$	1590	1575	Nujol	25
Sm$_2$(NHAr)$_6$	1590	1572	benzene	25
La(NHAr)$_3$(THF)$_3$	1588		Nujol	this work
La(NHAr)$_3$(py)$_2$	1588		Nujol	this work
KNHAr	1581		Nujol	this work
H$_2$NAr	1588		neat	this work
Aryloxides				
La$_2$(OAr)$_6$	1588	1571	Nujol	27
La$_2$(OAr)$_6$	1588	1572	benzene	27
Nd$_2$(OAr)$_6$	1588	1571	Nujol	6
Nd$_2$(OAr)$_6$	1590	1572	benzene	6
Sm$_2$(OAr)$_6$	1586	1572	Nujol	6
Sm$_2$(OAr)$_6$	1589	1572	benzene	6
Er$_2$(OAr)$_6$	1590	1571	Nujol	6
Er$_2$(OAr)$_6$	1589	1572	benzene	6
U$_2$(OAr)$_6$	1588	1553	Nujol	29
La(OAr)$_3$(THF)$_2$	1587		Nujol	27
Pr(OAr)$_3$(THF)$_2$	1584		Nujol	6
Nd(OAr)$_3$(THF)$_2$	1585		Nujol	6
Sm(OAr)$_3$(THF)$_2$	1585		Nujol	6
Gd(OAr)$_3$(THF)$_2$	1585		Nujol	6
Er(OAr)$_3$(THF)$_2$	1586		Nujol	6
Yb(OAr)$_3$(THF)$_2$	1586		Nujol	6
Lu(OAr)$_3$(THF)$_2$	1586		Nujol	6
La$_2$(OAr)$_6$(NH$_3$)$_2$	1583		Nujol	27
KLa(OAr)$_4$	1581		Nujol	79
LiOAr	1584		Nujol	27
HOAr	1585		neat	27

pyridine ν(C=C) modes, one at 1568 (IR) and 1569 (Raman) and another at 1594 cm^{-1} (IR and Raman)[36–38] and one ν(C=C) mode predominantly from the arylamido ligand (IR = 1588 cm^{-1}; Raman = 1589 cm^{-1}). This latter peak may be broadened by the pyridine mode, but the single-peak structure from the arylamido ligand is consistent with the terminal nature of the ligand. These arylamido ν(C=C) modes for the monomeric THF and pyridine adducts of the arylamide compare favorably with that determined for the monomeric aryloxide species, La(OAr)$_3$(THF)$_2$ (1587 cm^{-1}).[27]

Of significance is that the IR spectrum of **1** recorded in benzene solution also shows two ν(C=C) frequencies at 1588 and 1572 cm^{-1}, suggesting the solid-state η^6-arene-bridged structure (**I**) is maintained in solution. Although a dimeric

X = O, NH

I   **II**
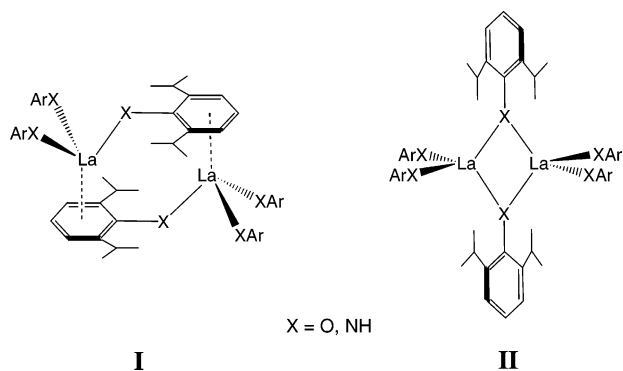
structure involving arylamido ligands bridging through nitrogen would also possess two types of arylamido ligands (**II**), the ν(C=C) stretching frequencies in this case would be expected

to be so similar that they would not be resolved as two distinct bands. This is the case for the oxygen-bridged complex La$_2$(μ-O-2,6-^{i}Pr$_2$OC$_6$H$_3$)$_2$(O-2,6-^{i}Pr$_2$OC$_6$H$_3$)$_4$(NH$_3$)$_2$,[27] which shows only a single set of ν(C=C) vibrational modes at 1583 cm^{-1} by IR spectroscopy. Thus the combination of IR and Raman spectroscopy clearly indicate that the π-arene bridge is maintained in both the solid state and in solution. This understanding gleaned from the vibrational spectra is important for our interpretation of solution behavior monitored by ^{1}H NMR spectroscopy.

B. Room-Temperature ^{1}H NMR Spectroscopy. The ^{1}H NMR spectrum of **1** recorded under ambient conditions reveals arylamido groups in a 2:1 ratio, consistent with the presence of one bridging and two terminal -NHAr groups per metal center. The NH protons appear as two broad singlets of 1:2 ratio at 5.37 and 5.12 ppm, consistent with our interpretation (vibrational spectroscopy) that the π-arene-bridged dimeric structure is maintained in solution. Despite the presence of diastereotopic methyl groups in **1**, we were only able to observe a single resonance arising from the isopropyl methyl groups of the terminal arylamido groups. The results of variable-temperature ^{1}H NMR studies of this compound and its aryloxide congener will be presented later.

The room-temperature ^{1}H NMR spectrum of **2** in d_8-THF is consistent with a monomeric Lewis base adduct in solution. The spectrum shows one type of arylamido ligand and one type of THF ligand environment in a 1:1 ratio, indicative of the formation of a tris-THF adduct which adopts either a static *fac*-octahedral geometry in solution or possesses a *mer* geometry with ligands rapidly equilibrating on the NMR time scale.

Monitoring the stepwise addition of THF to La$_2$(NHAr)$_6$ (**1**) by ^{1}H NMR reveals the disappearance of resonances arising from dimeric **1** and the growth of peaks due to the tris-THF complex **2**. Figure 5a shows the results of the addition of between 1 and 6 equiv of THF to La$_2$(NHAr)$_6$ (**1**) in C$_6$D$_6$. For the sake of clarity, only the arylamido NH region of the spectra is shown. The initial spectrum consists of two peaks in a 2:1 ratio at 5.37 (**A1**) and 5.12 ppm (**A2**), consistent with the presence of La$_2$(NHAr)$_6$ (**1**) only. As THF is added to the sample, these signals due to **1** decrease in intensity, while the resonance at 5.08 ppm (**B**), corresponding to the tris-THF adduct La(NHAr)$_3$(THF)$_3$ (**2**), grows in. Additionally, a small peak at 5.28 ppm (**C**) is also observed. We suggest that this peak arises from the presence of a small quantity of the more traditional nitrogen-bridged dimer La$_2$(μ-NHAr)$_2$(NHAr)$_4$(THF)$_2$ (**III**) illustrated in Scheme 1. We have previously shown that the addition of NH$_3$ to the π-arene-bridged aryloxide dimer La$_2$(OAr)$_6$ to form the tetra-ammonia adduct La(OAr)$_3$(NH$_3$)$_4$ passes through the oxygen-bridged aryloxide dimer La$_2$(μ-OAr)$_2$-(OAr)$_4$(NH$_3$)$_2$.[27] It may be that a similar interconversion is present in this case, although we note that we were unable to isolate La$_2$(μ-NHAr)$_2$(NHAr)$_4$(THF)$_2$ (**III**) free from other arylamido-containing species, and thus the assignment of the peak at 5.28 ppm in the ^{1}H NMR spectrum to this complex remains speculative at this time (Scheme 1).

Interestingly, the addition of THF to the arylamido-bridged dimer **1** is reversible; if a solid sample of the tris-THF adduct

(36) Kline, C. H.; Turkevich, J. *J. Chem. Phys.* **1944**, *12*, 300.
(37) Wilmshurst, J. K.; Bernstein, H. J. *Can. J. Chem.* **1957**, *35*, 1183.
(38) Nakamoto, K. *Infrared and Raman Spectra of Inorganic and Coordination Compounds*, 4th ed.; Wiley-Interscience: New York, 1986.
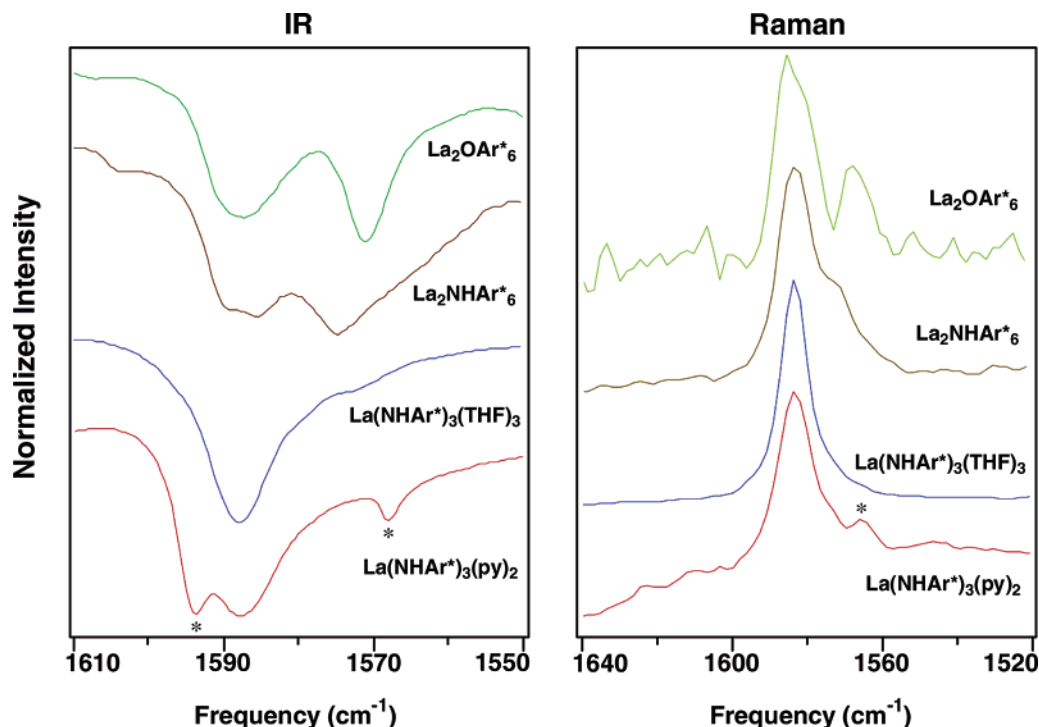
IR

Raman

Figure 4. $v(C=C)$ stretching region of the solid-state infrared (left) and Raman (right) spectra of La$_2$(O-2,6-^{i}Pr$_2$C$_6$H$_3$)$_6$ (**4**), La$_2$(NH-2,6-^{i}Pr$_2$C$_6$H$_3$)$_6$ (**1**), La(NH-2,6-^{i}Pr$_2$C$_6$H$_3$)$_3$(THF)$_3$ (**2**), and La(NH-2,6-^{i}Pr$_2$C$_6$H$_3$)$_3$(py)$_2$ (**3**) (top to bottom). Asterisk denotes peaks arising from pyridine solvent.

2 is dissolved in toluene and subjected to prolonged exposure to vacuum, compound **1** is obtained. The results of this ^{1}H NMR experiment are shown in Figure 5b. The initial sample of La(NHAr)$_3$(THF)$_3$ (**2**) reveals a single peak at 5.08 ppm (**B**); exposure of this sample to vacuum for 12 h results in the regeneration of peaks at 5.37 and 5.12 ppm (**A1** and **A2**), consistent with the re-formation of the π-arene-bridged dimer **1**. This type of behavior has not been reported for the aryloxide derivative, for which adduct formation with THF or pyridine is irreversible.[27] Interestingly, after 3 h under dynamic vacuum, the dimer **1** and the tris-THF adduct **2** are visible, as well as the purported nitrogen-bridged dimer La$_2$(μ-NHAr)$_2$(NHAr)$_4$-(THF)$_2$ (**III**), lending further credence to the interconversion postulated in Scheme 1.

The room-temperature ^{1}H NMR spectrum of **3** in d_5-pyridine is consistent with expectations for a monomeric complex; the spectrum reveals a single type of arylamido group in solution. The addition of pyridine to compound **1** does not appear to be reversible, as exposure of a d_8-toluene solution of **3** to vacuum does not result in any change in the ^{1}H NMR spectrum. In this sense, the bis-pyridine adduct **3** behaves more like the aryloxide species La(OAr)$_3$(THF)$_2$ and La(OAr)$_3$(py)$_3$, for which solvent loss was not observed.

C. Variable-Temperature NMR Spectroscopy. 1. Aryloxide System. In view of the structural similarities between the arylamide dimer La$_2$(NH-2,6-^{i}Pr$_2$C$_6$H$_3$)$_6$ reported here and the related aryloxide La$_2$(O-2,6-^{i}Pr$_2$C$_6$H$_3$)$_6$ (**4**) reported previously, we were interested in exploring the relative effect that arylamide versus aryloxide substituents would have on the solution behavior. Thus, we undertook a more detailed study of compound **4** in order to determine the kinetic parameters associated with the fluxional process operative in solution.

Figure 6 shows a stacked plot of the isopropyl methyl region of the ^{1}H NMR spectra of **4** in C$_7$D$_8$ solution at temperatures

ranging from 0 to 60 °C. In general, the isopropyl methyl groups appear as doublets due to coupling to a single methine proton. At high temperature, all of the isopropyl methyl groups are averaged to give a single doublet at 1.25 ppm, indicating a rapid bridge−terminal ligand exchange process. Cooling the sample results in decoalescence and a slowing of the exchange process until two doublets of 2:1 intensity at 1.29 and 1.17 ppm are frozen out at 0 °C, suggesting that a dimeric structure is retained in solution. Line-shape analysis allowed for the extraction of exchange rate constants at various temperatures; the subsequent Arrhenius plot yielded activation parameters of $\Delta G^{\ddagger} = 14.4$ kcal mol^{-1}, $\Delta S^{\ddagger} = 5$ cal K^{-1} mol^{-1}, $\Delta H^{\ddagger} = 16.0$ kcal mol^{-1}, and $E_a = 16.5$ kcal mol^{-1}. The slightly positive value of $\Delta S^{\ddagger}$ implies that the aryloxide ligands are averaged via a dissociative transition state, although the small value of $\sim$5 cal K^{-1} mol^{-1} suggests only a minimal rearrangement occurs. This allows us to propose a possible mechanism by which the bridging and terminal ligands are exchanged, as well as discount other possibilities. One possibility is that the dimer breaks apart into two monomeric units and rapidly re-forms in solution; this would account for the averaging of all three aryloxide ligands. However, there is no evidence by ^{1}H NMR spectroscopy for a monomer−dimer equilibrium. A second possible means of exchange is outlined in Scheme 2, whereby the π-arene-bridged dimer converts to a dimeric species which is bridged via the aryloxide oxygen atoms; such a structure has been observed for the Lewis base stabilized complex La$_2$(μ-O-2,6-^{i}Pr$_2$C$_6$H$_3$)$_2$-(O-2,6-^{i}Pr$_2$C$_6$H$_3$)$_4$(NH$_3$)$_2$[27] as well as other f-element complexes such as Th$_2$(OCH-i-Pr$_2$)$_8$[15] and U$_2$(NEt$_2$)$_8$.[39] However, the mechanism presented in Scheme 2 does not exchange the bridge and terminal aryloxide groups, but only the metal center with which the bridging aryloxide group is interacting.

(39) Reynolds, J. G.; Zalkin, A.; Templeton, D. H.; Edelstein, N. M.; Templeton, L. K. *Inorg. Chem.* **1976**, *15*, 2498.
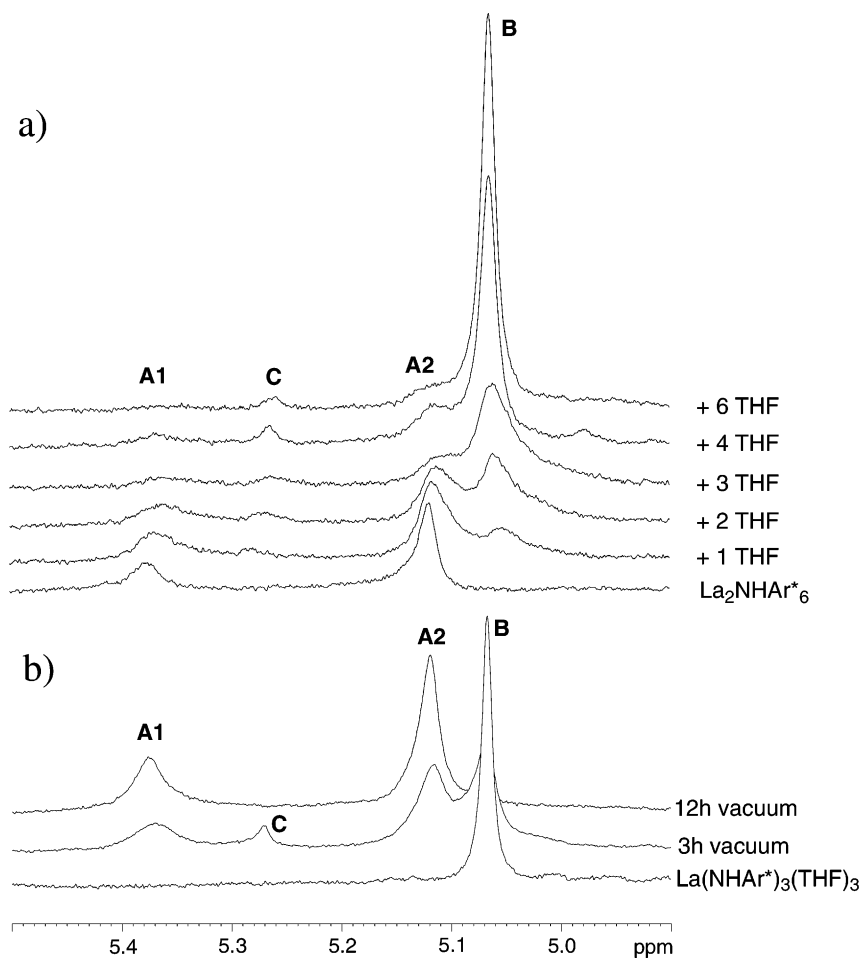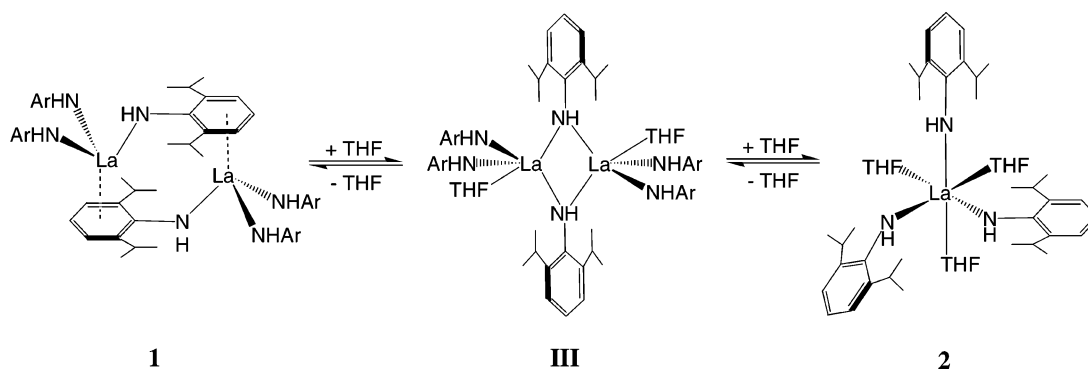
Figure 5. (a) 500.13 MHz ¹H NMR spectra of the arylamido NH region of La₂(NH-2,6-ⁱPr₂C₆H₃)₆ (**1**) upon addition of THF. (b) 500.13 MHz ¹H NMR spectra of the arylamido NH region of La(NH-2,6-ⁱPr₂C₆H₃)₃(THF)₃ (**2**) upon exposure to vacuum.

Scheme 1

It is also possible that an intermediate involving more than two oxygen-bridged aryloxide groups is involved (Scheme 3). This would allow for bridging and terminal groups to be exchanged; however, this may be discounted on the basis of the large negative value of $\Delta S^{\ddagger}$ that would be expected for such an ordered transition state.

Scheme 4 reveals a mechanism that is consistent with all of the experimental data. In this mechanism, (a) one of the π-arene interactions between a lanthanum metal center (La1) and a bridging aryloxide group (O1) is cleaved, while the other metal−π-arene bond within the dimer remains intact, (b) the La(OAr)₃ unit rotates 120° about the La2−arene bond, and (c) an aryloxide group which was originally in a terminal

position (O3) re-coordinates to La1, with a new π-arene interaction becoming a bridging aryloxide unit. The transition state for this exchange is only minimally more disordered than the starting dimer, consistent with the small positive value of $\Delta S^{\ddagger}$. Although we have only shown the exchange involving one lanthanum center, the same dissociation−rotation−reassociation can also occur at the second metal site. If this mechanism is operative in this complex, the $\Delta H^{\ddagger}$ value of 16.0 kcal mol⁻¹ corresponds to the energy required to break the π-arene bond. This number correlates well with theoretical calculations of the strength of such interactions in model compounds containing a benzene ring bound in an η^6-manner to a lanthanide center (see later).

2. Arylamide System. The variable-temperature ^{1}H NMR spectra of La$_2$(NH-2,6-^{i}Pr$_2$C$_6$H$_3$)$_6$ (**1**) also show evidence for fluxional behavior. The isopropyl methyl region of the ^{1}H NMR spectra of **1** show the same basic features as those found for the aryloxide derivative **4**, although the coalescence of two doublets (1.31 and 1.26 ppm) to one doublet (1.29 ppm) occurs between 25 and 90 °C, approximately 30° higher than that for compound **4**. As for compound **4**, line-shape analysis and the subsequent Arrhenius plot yielded activation parameters: $\Delta G^\ddagger$ = 15.1 kcal mol^{-1}, $\Delta S^\ddagger$ = 24 cal K^{-1} mol^{-1}, $\Delta H^\ddagger$ = 22.5 kcal mol^{-1}, and E_a = 23.1 kcal mol^{-1}. The positive value of $\Delta S^\ddagger$ suggests that the bridging and terminal arylamido ligands are averaged by a dissociative mechanism. However, the value determined for the arylamide system is much larger than that observed for the aryloxide species (24 vs 5 cal K^{-1} mol^{-1}). Thus, it is unlikely that the same mechanism is operative in the two systems. In the arylamido case, it is probable that the dimer breaks apart into two monomers (eq 4) and randomly re-forms, which would average the arylamido groups between the bridging and terminal positions. This postulate is supported by the observation of a monomer−dimer equilibrium at elevated temperatures, which was not found for **4** (see later). One must be careful when comparing $\Delta S^\ddagger$ values, since these numbers are small and subject to considerable error. We determined the error in this parameter to be approximately 5 cal K^{-1} mol^{-1}; thus we can say with some certainty that both systems involve a mechanism with a transition state that is more disordered than the reactants. Also, despite the error associated with $\Delta S^\ddagger$, it appears that the fluxionality occurring in the arylamido complex **1** involves a more disordered transition state than the aryloxide complex **4** and therefore a different mechanism.

In addition to the fluxional behavior described above, at elevated temperatures there is evidence for an equilibrium between dimeric La$_2$(μ-NH-2,6-^{i}Pr$_2$C$_6$H$_3$)$_6$ (**1**) and a monomeric species such as La(NH-2,6-^{i}Pr$_2$C$_6$H$_3$)$_3$ (eq 4). Figure 7 shows a
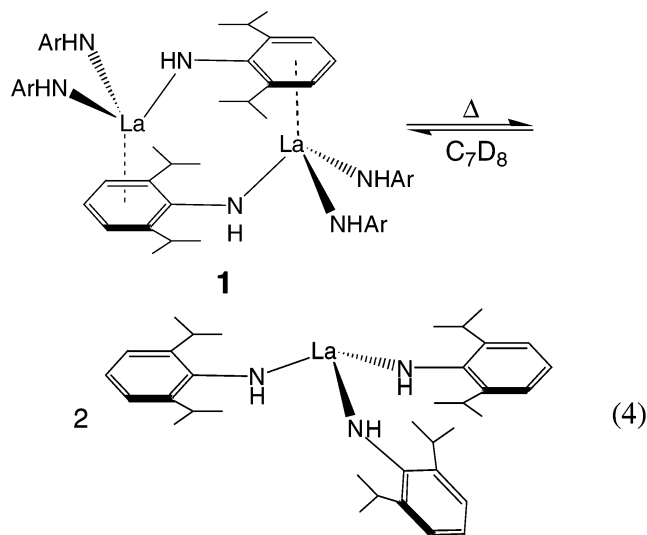
stacked plot of the ^{1}H NMR spectrum of **1** in C$_7$D$_8$ solution at temperatures from 25 to 90 °C, in which the arylamido NH region of the spectra have been expanded. At room temperature, two broad singlets of ratio 1:2 are visible at 5.35 (**A1**) and 5.08 ppm (**A2**), due to the bridging and terminal aryl-
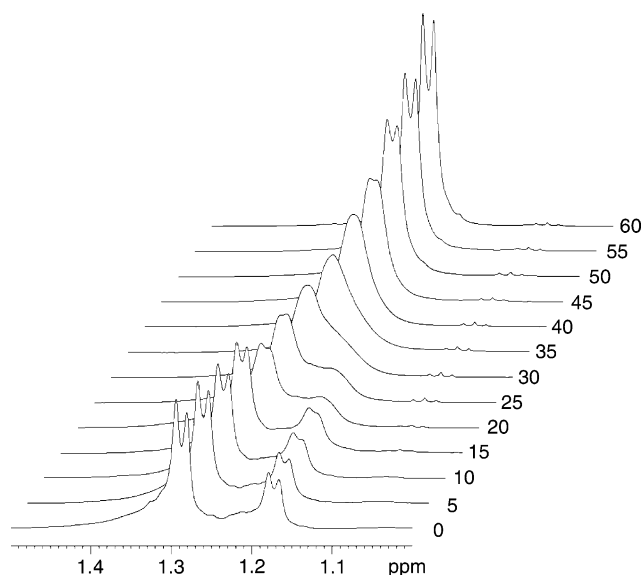
Figure 6. Variable-temperature 500.13 MHz ^{1}H NMR spectra of the isopropyl methyl region of La$_2$(O-2,6-^{i}Pr$_2$C$_6$H$_3$)$_6$ (**4**).

amido groups, respectively. As the temperature is increased, a third peak at 4.73 ppm (**D**) grows in. We suggest that this peak arises from the monomeric species La(NH-2,6-^{i}Pr$_2$C$_6$H$_3$)$_3$, which contains only one type of arylamido group. As the sample is heated, resonances assigned to the dimer **1** are seen to decrease, while those resulting from the monomer are observed to increase, although even at 90 °C the dimer **1** is still the predominant species in solution. When cooled back to room temperature, the resonances of the monomer quickly disappear until only the dimer is visible, implying a low barrier to dimerization.

We note that as the temperature is increased to 50 °C, the NH peak at 5.35 ppm (**A1**) appears to separate into a broad resonance at 5.40 ppm and a smaller, sharper peak at 5.46 ppm. This suggests that a further equilibrium and/or dynamic process may be occurring in addition to the monomer−dimer equilibrium proposed in eq 4. Although the process that gives rise to this splitting was not investigated, we believe the presence of this minor peak has a minimal effect on the calculation of thermodynamic parameters for this system, and the equilibrium described in eq 4 is the major mode by which the bridging and terminal groups are exchanged.

To confirm that peak **D** in Figure 7 corresponds to a monomeric species such as La(NHC$_6$H$_3^i$Pr$_2$-2,6)$_3$, we also obtained an ^{1}H NOESY NMR spectrum of the sample (Figure 8). To observe any possible exchange between the dimer **1** (peaks **A1** and **A2** in Figure 7) and a monomeric lanthanum arylamido species (peak **D** in Figure 7), we performed the experiment at 45 °C, where all three resonances were visible in the 1D ^{1}H NMR spectrum. The presence of large cross-peaks between the resonances at 5.45 (**A1**) and 5.19 (**A2**) ppm confirms that rapid bridge−terminal exchange occurs within the dimer at this temperature. Also, small cross-peaks are visible between the resonance at 4.90 ppm (**D**, monomer) and those at 5.45 and 5.19 ppm, indicating that the arylamido groups of monomeric La(NH-2,6-^{i}Pr$_2$C$_6$H$_3$)$_3$ exchange with both the bridging and terminal positions of the arylamido groups in La$_2$(NH-2,6-^{i}Pr$_2$C$_6$H$_3$)$_6$ (**1**), supporting the existence of a monomer−dimer equilibrium in solution.
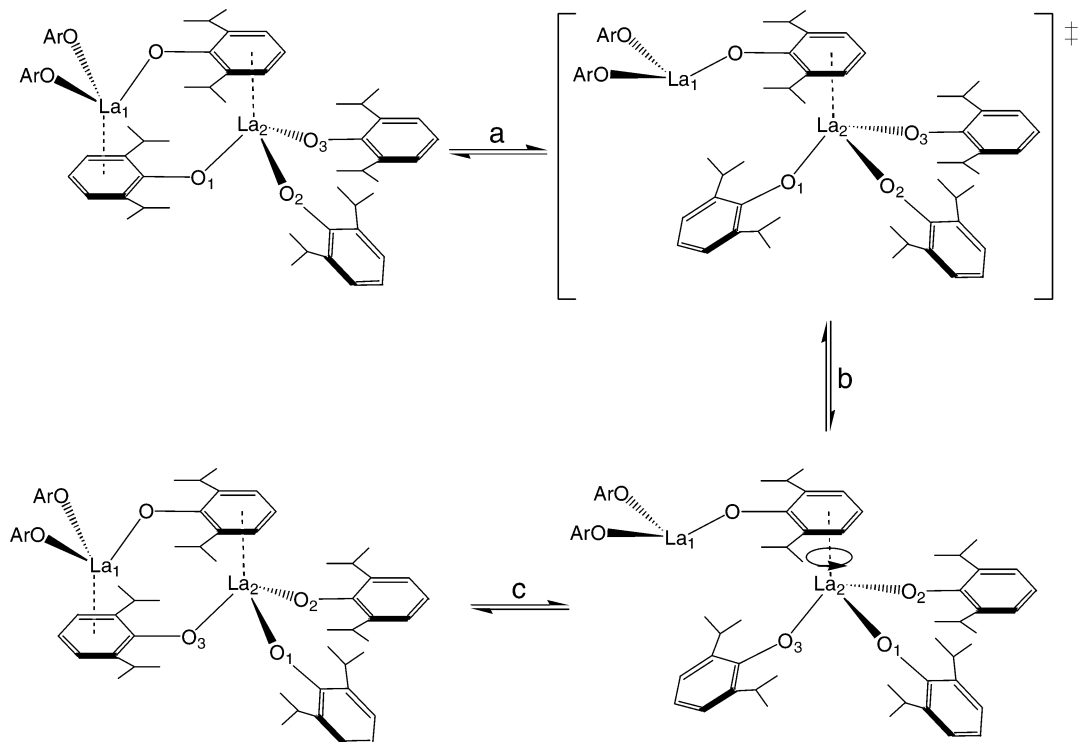
Scheme 2
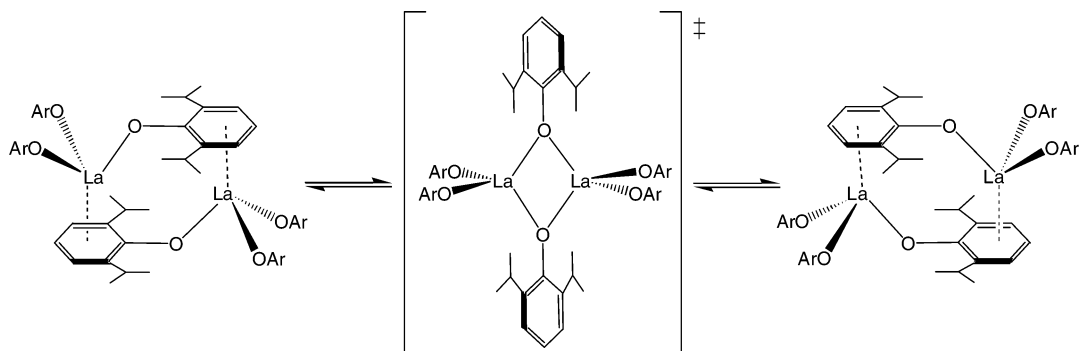
Scheme 3
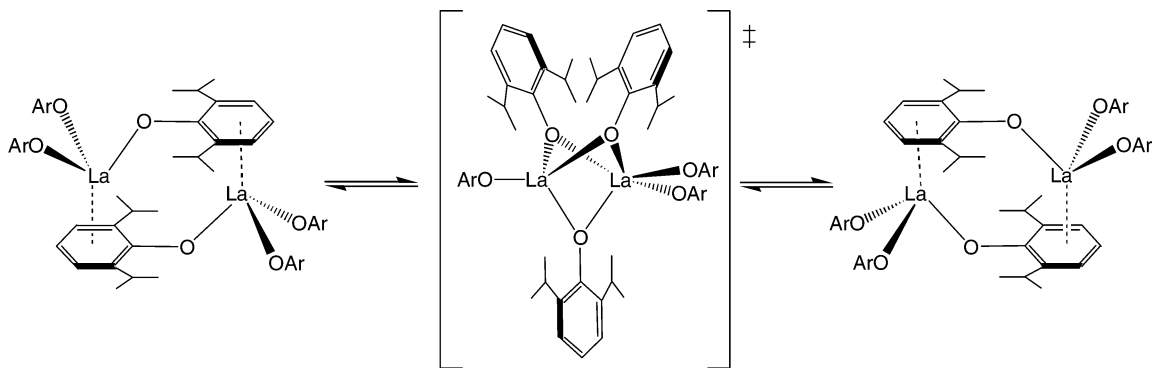
Scheme 4

Thermodynamic parameters for the equilibrium were determined by measuring the relative concentrations of monomer and dimer over a range of temperatures. A plot of $\ln(K_{eq})$ vs $1/T$ yielded the following parameters: $\Delta H° = 20$ kcal mol^{-1}, $\Delta G°_{298} = 4$ kcal mol^{-1}, $\Delta S° = 55$ cal K^{-1} mol^{-1}, and $K_{eq}^{298} = 1.19 \times 10^{-3}$. These values may be compared with those found for the monomer−dimer equilibrium process for the thorium

alkoxide complex shown in eq 5, in which $\Delta H° = 17$ kcal mol^{-1}, $\Delta G°_{298} = 5$ kcal mol^{-1}, and $\Delta S° = 40$ cal K^{-1} mol^{-1}.[15]

$$Th_2(OCH^iPr_2)_8 \rightleftharpoons 2\ Th(OCH^iPr_2)_4 \qquad (5)$$
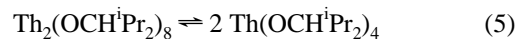
In comparing the two systems, both the entropy and enthalpy terms are found to be similar for the two equilibria. The close

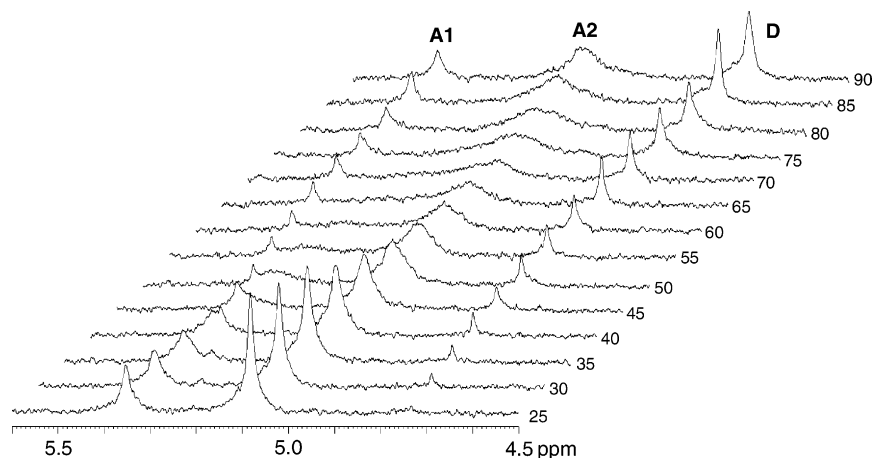**Figure 7.** Variable-temperature 500.13 MHz ^{1}H NMR spectra of the arylamido NH region of La$_2$(NH-2,6-^{i}Pr$_2$C$_6$H$_3$)$_6$ (**1**).
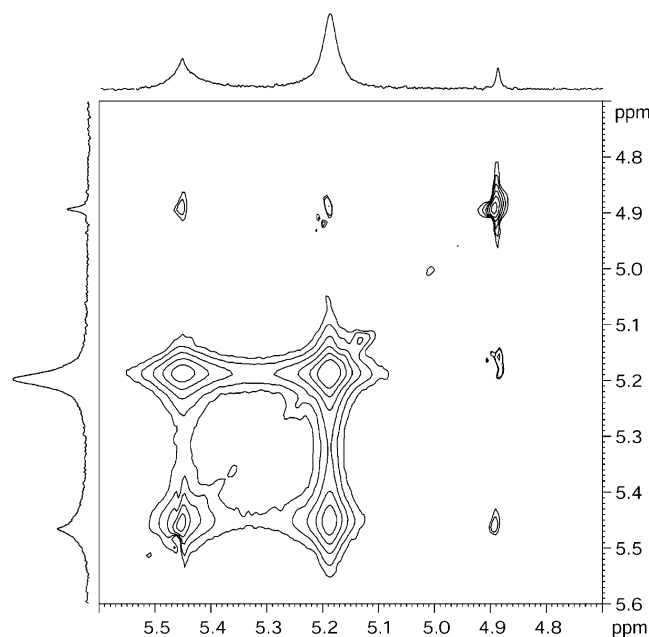
Figure 8. 500.13 MHz ^{1}H NOESY spectrum of the arylamido NH region of La$_2$(NH-2,6-^{i}Pr$_2$C$_6$H$_3$)$_6$ (**1**) in C$_7$D$_8$ at 318 K indicating bridge–terminal exchange and monomer–dimer equilibrium.

correlation of the entropy change may be explained by the similarity of the structures of the thorium and lanthanum complexes. The enthalpy values for the two systems are also within the same range (20 kcal mol^{-1} for La; 17 kcal mol^{-1} for Th), implying that the π-arene bridging mode is energetically similar to the alkoxide-bridged structure observed for Th$_2$(OCH^{i}Pr$_2$)$_8$. Thus, it is interesting that no comparable monomer–dimer equilibrium is observed for the aryloxide complex La$_2$(μ-O-2,6-^{i}Pr$_2$C$_6$H$_3$)$_6$ (**4**), which remains dimeric (**I**) at all temperatures under study. Additionally, there is never evidence that complex **4** bridges through the aryloxide oxygen atoms (**II**) by variable-temperature ^{1}H NMR spectroscopy. Thus, the π-arene interaction in La$_2$(O-2,6-^{i}Pr$_2$C$_6$H$_3$)$_6$ (**4**) must be stronger than the analogous interaction observed in the arylamido derivative La$_2$(NH-2,6-^{i}Pr$_2$C$_6$H$_3$)$_6$ (**1**).

The thermodynamic parameters presented for compound **1** also suggest that the bridging and terminal arylamido groups are only exchanged as a result of a monomer–dimer equilib-

rium, i.e., a mechanism such as that outlined in Scheme 4 is not valid for compound **1**. The observation of similar values of $\Delta H°$ (20 kcal mol^{-1}) and $\Delta H^‡$ (22.5 kcal mol^{-1}) for the formation of a dative bond with a neutral donor implies that the exchange of bridging and terminal arylamido groups occurs through a single pathway.

IV. Theoretical Calculations. A. Structural Results. The experimental studies indicate that the relative strength of the La–η-arene bonds follow the order OAr > NHAr. To gain a better understanding of the nature of the π-arene interactions in compounds **1** and **4**, DFT calculations were carried out on simplified model complexes La$_2$(OC$_6$H$_5$)$_6$, La$_2$(NHC$_6$H$_5$)$_6$, and (C$_6$H$_5$R)La(XC$_6$H$_5$)$_3$, where X = O or NH and R = H, OH or NH$_2$. Remarkably, the geometry optimization of the model dimers using the B3YLP functional produced π-arene-bridged geometries for both systems. The calculated structures of the model dimer complexes La$_2$(μ-NHPh)$_2$(NHPh)$_4$ and La(μ-OPh)$_2$-(OPh)$_4$ are shown in Figure 9, and the relevant calculated structural parameters are given in Table 6. While the calculations reproduce the overall experimental structures, the bond lengths are all slightly overestimated. Larger differences are noted in the La–C contacts of the π-arene groups, where the average La–C distance is overestimated by ~0.13 Å in the arylamide complex and ~0.15 Å in the aryloxide complex. The interactions involving the π-arene moieties will be discussed below.

B. Electronic Structure. The principal metal–ligand bonding interaction in three-coordinate lanthanide LnX$_3$ complexes arises from a σ bonding interaction between occupied ligand lone pair orbitals and empty metal 5d, 6s, and 6p acceptor orbitals. As discussed in previous papers on tris-amide and tris-alkyl complexes,[25,40–44] the resultant metal–ligand bond is variously described as ranging from highly polar to ionic with the lanthanide ion having significant positive charge. In addition, for both tris-amide and tris-arylamide complexes, there is also a π lone pair orbital on the nitrogen ligand. The σ and π symmetry frontier orbitals of the NHPh ligand are shown

(40) Maron, L.; Eisenstein, O. *J. Phys. Chem. A* **2000**, *104*, 7140.
(41) Maron, L.; Eisenstein, O. *New J. Chem.* **2001**, *25*, 255.
(42) Perrin, L.; Maron, L.; Eisenstein, O.; Lappert, M. F. *New J. Chem.* **2003**, *27*, 121.
(43) Clark, D. L.; Gordon, J. C.; Hay, P. J.; Martin, R. L.; Poli, R. *Organometallics* **2002**, *21*, 5000.
(44) Brady, E. D.; Clark, D. L.; Gordon, J. C.; Hay, P. J.; Keogh, D. W.; Poli, R.; Scott, B. L.; Watkin, J. G. *Inorg. Chem.* **2003**, *42*, 6682.
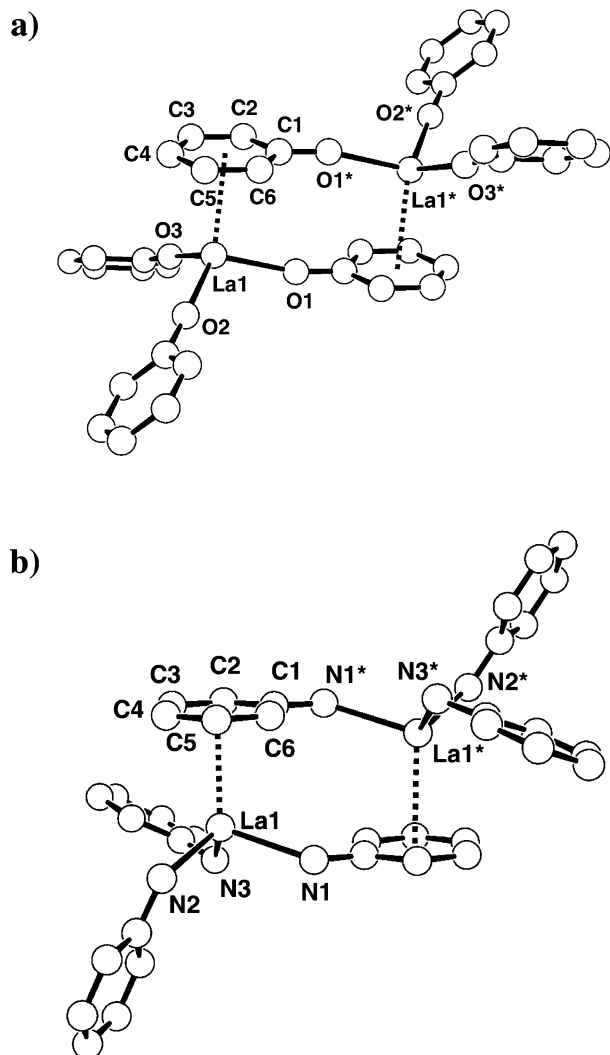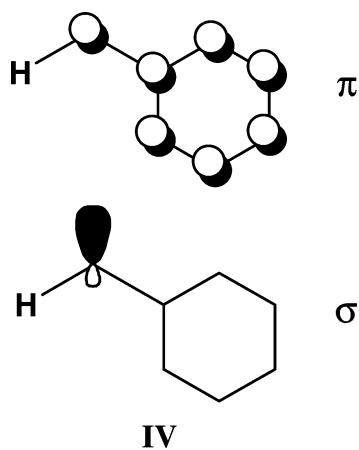
a)

b)

Figure 9. Views of the fully optimized (a) La$_2$(μ-OPh)$_2$(OPh)$_4$ and (b) La$_2$(μ-NHPh)$_2$(NHPh)$_4$ structures from B3LYP calculations.

schematically in **IV**, where conjugation with the π electrons of the benzene ring is depicted.

IV

In the DFT calculations on the La(NHPh)$_3$ monomer, the overall charge on the La atoms is calculated as +1.47 (i.e., much less ionic than the formal oxidation state of +3) that gives orbital populations of (6s,6p)$^{0.24}$5d$^{1.29}$ for La from the standard Mulliken analysis (Table 7). The coordinatively unsaturated monomer can

Table 6. Comparison of Selected Calculated and Experimental Structural Parameters for La$_2$(XAr)$_6$ (X = O, NH; Ar = 2,6-^{i}Pr$_2$C$_6$H$_3$ (exp), Ph (calc))

	experimental	calculated
	La$_2$(μ-NHAr)$_2$(NHAr)$_4$	La$_2$(μ-NHPh)$_2$(NHPh)$_4$
La−N$_{terminal}$	2.347, 2.360 Å	2.367, 2.375 Å
La−N$_{bridging}$	2.434 Å	2.472 Å
La−C$_{arene}$	2.972−3.209 Å	3.186−3.248 Å
N$_{terminal}$−La−N$_{terminal}$	122.3	112.4
N$_{terminal}$−La−N$_{bridging}$	93.2, 111.2	102.5, 104.9
	La$_2$(μ-OAr)$_2$(OAr)$_4$	La$_2$(μ-OPh)$_2$(OPh)$_4$
La−O$_{terminal}$	2.187, 2.197 Å	2.219, 2.221 Å
La−O$_{bridging}$	2.273 Å	2.312 Å
La−C$_{arene}$	2.978−3.164 Å	3.133−3.310 Å
O$_{terminal}$−La−O$_{terminal}$	106.4	110.5
O$_{terminal}$−La−O$_{bridging}$	112.7, 115.2	108.2, 112.7

Table 7. Calculated Lanthanum Metal Charge and Mulliken Orbital Populations

	charge (La)	6s,6p (e$^-$)	5d (e$^-$)
La(NHPh)$_3$	+1.47	0.24	1.29
La(NHPh)$_3$(η^6-C$_6$H$_5$R)	+1.32	0.44	1.24
La$_2$(μ-NHPh)$_2$(NHPh)$_4$	+1.33	0.38	1.29
La$_2$(μ-OPh)$_2$(OPh)$_4$	+1.44	0.40	1.16

accept π-donation from the benzene ring in the series of model complexes (η^6-C$_6$H$_5$R)La(NHPh)$_3$ (R = H, OH, NH$_2$) discussed below or from one of the bridging NHPh ligands in the dimeric complex La$_2$(μ-η^6-NHPh)$_2$(NHPh)$_4$. The overall charge on the La has been reduced slightly to +1.32 and +1.33 for (η^6-C$_6$H$_5$R)La(NHPh)$_3$ and La$_2$(μ-η^6-NHPh)$_2$(NHPh)$_4$, respectively. The 5d population remains relatively unchanged with slight increases of 0.20 and 0.14 e$^-$ in the 6s,6p populations (respectively) as a result of interaction with an η^6-arene unit. Some of the key molecular orbitals are shown in Figure 10 for the case of (η^6-C$_6$H$_6$)La(NHPh)$_3$. Relatively little change in energy is evident for the highest occupied molecular orbitals arising from the π lone pair orbitals of NHPh, for example. The major changes are the stabilization of the occupied benzene π-bonding orbitals upon complexation to La(NHPh)$_3$, by 0.06 au for the highest occupied benzene π-bonding orbital (e$_{1g}$) and 0.104 au for the totally symmetric benzene π-bonding orbital (a$_{2u}$) upon complexation. However, there is very little metal admixture into these orbitals in the (η^6-C$_6$H$_6$)La(NHPh)$_3$ molecular orbitals. Comparing La$_2$(μ-η^6-OPh)$_2$(OPh)$_4$ to La$_2$(μ-η^6-NHPh)$_2$(NHPh)$_4$, the La atoms are slightly more electropositive in the aryloxide derivative (+1.44 vs +1.33) with somewhat smaller 5d populations (1.16 e$^-$ vs 1.24 e$^-$). The DFT calculations suggest that the metal−ligand σ-bonding in the LnX$_3$ unit takes place primarily through interaction with La 5d orbitals, while the metal−π-arene interaction takes place primarily through the 6s/6p manifold.

C. Thermochemistry. The experimentally observed differences in solution behavior and coordination chemistry between the arylamide and aryloxide dimers led us to examine the relative magnitude of π-bonding interactions with La(XPh)$_3$ units (X = O, NH). We recall that the arylamide dimer La$_2$(NHAr)$_6$ (**1**) reacts *reversibly* with THF to form La(NHAr)$_3$(THF)$_3$ (**2**), while the analogous reactivity for the aryloxide complex La$_2$(OAr)$_6$ (**4**) is *irreversible*. The two π-arene-bridged dimers also exhibit different NMR behavior (vide infra) in which the former complex appears to break apart into monomeric units in solution
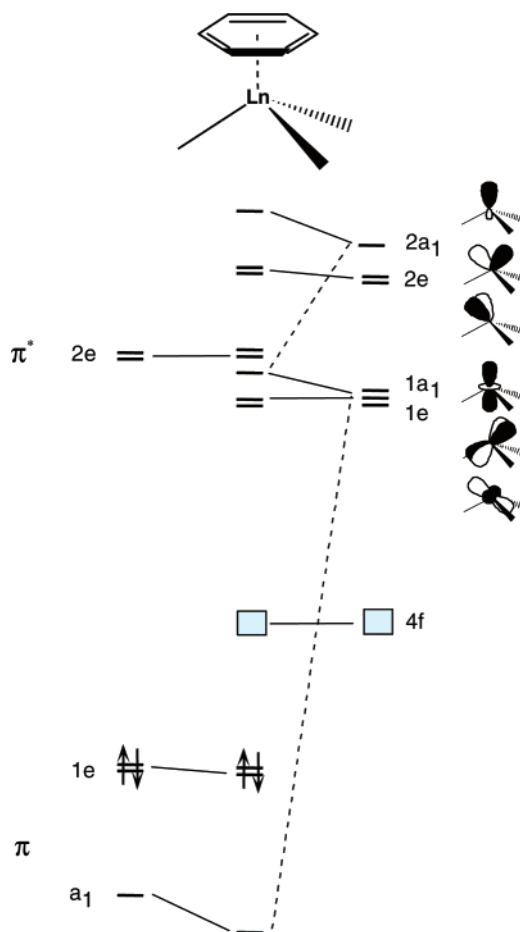
Figure 10. Orbital energies of selected molecular orbitals in C_6H_6 (left), $(\eta^6\text{-}C_6H_6)La(NHAr)_3$ (center), and $La(NHAr)_3$ (right) from DFT calculations.

while the latter loses only one π-bonding interaction under similar conditions.

The calculated energy of forming the dimeric species was determined from the calculated structures of both monomeric $La(XPh)_3$ and dimeric $La_2(XPh)_6$ for each species (X = O, NH) as given in Table 8. While the dimer formation is energetically favored in both cases (-48.1 kcal mol^{-1} for $La_2(OPh)_6$, -45.1 kcal mol^{-1} for $La_2(NHPh)_6$), the aryloxide forms the slightly stronger π-arene interaction by about 3 kcal mol^{-1}. To further isolate the nature of the π-arene interaction, the binding of a sequence of benzene, phenol, and aniline to $La(XPh)_3$ monomers (X = O, NH) was examined to form the hypothetical monomer $(\eta^6\text{-}C_6H_5R)La(XPh)_3$ (**V**) (X = O, NH; R = H, OH, NH$_2$). As


V
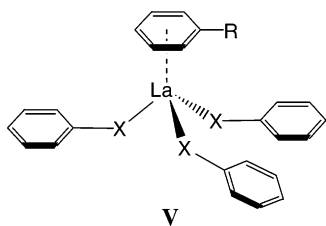
shown in Table 8, all of the binding energies for the formation of a π-arene interaction lie in the vicinity of 15–22 kcal mol^{-1}, suggesting that the interactions in the dimer should be $\sim$30–45 kcal mol^{-1}. The dimers themselves are calculated to be somewhat higher at 45–48 kcal mol^{-1}. The binding energies calculated for monomers **V** are qualitatively similar to the

Table 8. Calculated Interaction Energies of π-Bonded Complexes

	calculated binding energy (kcal mol^{-1})	
interaction	X = NH	X = O
$La(XPh)_3 + La(XPh)_3$	-45.1	-48.1
$La(XPh)_3 +$ benzene	-15.4	-17.1
$La(XPh)_3 +$ HOPh	-17.3	-19.7
$La(XPh)_3 + H_2NPh$	-19.3	-21.9

experimental value of $\Delta H^{\ddagger}$ of 16.0 kcal mol^{-1} obtained for the aryloxide-bridged dimer **4**, in which only one of the π-arene interactions was thought to be cleaved in solution. This number is similar to the value of 19.7 kcal mol^{-1} calculated for breaking the interaction between $La(OPh)_3$ and C_6H_5OH (the values in Table 8 are calculated for bond forming, not bond breaking). For each monomer **V**, the π-bonding interaction increases in the order benzene < phenol < aniline, and the π-arene interaction is stronger to $La(OPh)_3$ than $La(NPh)_3$. The slightly weaker affinity of arylamide complexes for π-arene ligands is consistent with the experimental results, but the relatively small, calculated energy changes are surprising in view of the drastically different solution chemistry.

The experimental enthalpy of activation, $\Delta H^{\ddagger}$, for ligand exchange in dimer **1** is 22.5 kcal mol^{-1} determined in toluene solution, which is low by a factor of 2 compared to the calculated value (45 kcal mol^{-1}, Table 8) and corresponds to each metal–arene bond being worth only 11 kcal mol^{-1}. In view of the calculated stabilization afforded to monomeric $La(NPh)_3$ by coordination of simple π-arenes such as benzene, we reevaluated our interpretation of the solution behavior of the arylamide dimer $La_2(NH\text{-}2,6\text{-}^iPr_2C_6H_3)_6$ (**1**). Indeed, the calculations suggest that we should consider the interaction of monomeric $La(NH\text{-}2,6\text{-}^iPr_2C_6H_3)_3$ with toluene solvent to form $(\eta^6\text{-}C_6H_5Me)La(NH\text{-}2,6\text{-}^iPr_2C_6H_3)_3$ of structure type **V** as a distinct possibility during the monomer–dimer equilibrium. The chemical equilibrium would take the form of eq 6.

$$La_2(NHAr)_6 + 2C_6H_5Me \rightleftharpoons 2(\eta^6\text{-}C_6H_5Me)La(NHAr)_3 \quad (6)$$
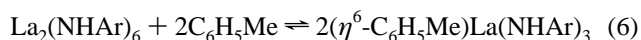
Using the data in Table 8, the reaction between $La_2(NHPh)_6$ and 2 equiv of benzene to give $(\eta^6\text{-}C_6H_6)La(NHPh)_3$ yields a reaction energy of 14.3 kcal mol^{-1}, in much better agreement with the experimental enthalpy of activation of 22.5 kcal mol^{-1} for ligand exchange in **1** determined in toluene solution. A structure containing a π-bound solvent molecule such as that described in eq 6 has been recently reported for the related complex $(\eta^6\text{-}C_6H_5Me)Nd[N(C_6F_5)_2]_3$,[45] although we were unable to conclusively determine if such an interaction was present in our system. For $La_2(O\text{-}2,6\text{-}^iPr_2C_6H_3)_6$ (**4**), we believe that only a single π-arene bond is cleaved (Scheme 4) and a dimeric structure is maintained in solution at all times; thus the interaction of the "uncomplexed" La center of the dimeric intermediate with a molecule of the toluene solvent is likely sterically disfavored.

F. Vibrational Frequencies. Vibrational frequencies were computed at the optimum geometries from the DFT calculations to aid in the interpretation of the experimental IR spectra of the various species present in solution. Since the IR peaks of most interest have been assigned to ring breathing modes, initial calculations on benzene were used to calibrate the DFT results.

(45) Click, D. R.; Scott, B. L.; Watkin, J. G. *Chem. Commun.* **1999**, 633.

Table 9. Calculated and Experimental Vibrational Frequencies Involving Ring-Breathing Modes of π-Arene Bridged Dimeric Complexes[a]

La$_2$(μ-OPh)$_2$(OPh)$_4$		La$_2$(μ-NHPh)$_2$(NHPh)$_4$	
calcd, cm^{-1} (rel intensity)	exptl, cm^{-1}	calcd, cm^{-1} (rel intensity)	exptl, cm^{-1}
1596, (0.21), t	1588 (solid), 1588 (soln)	1597, (0.34), t	1587 (solid), 1588 (soln)
1574, (0.40), br	1571 (solid), 1572 (soln)	1579, (0.94), br	1575 (solid), 1572 (soln)

[a] Calculated relative intensities and assignment of bridge (br) and terminal (t) rings are also shown. Calculated frequencies have been corrected as described in the text.

The two relevant modes in the 1400–1600 cm^{-1} spectral region are the IR-allowed e$_{1u}$ band observed at 1484 cm^{-1} and the Raman allowed e$_{2g}$ band at 1601 cm^{-1}. In the 6-31G basis set the B3LYP calculations predict these transitions to occur at 1541 and 1654 cm^{-1}, which are 57 and 53 cm^{-1} higher than experiment, respectively. Accordingly, in the La complexes the calculated harmonic frequencies were corrected by 55 cm^{-1} when compared with the observed bands.

With six phenyl rings in the dimeric complexes there will be one family of 12 vibrational transitions corresponding roughly to the six original e$_{1u}$ doubly degenerate benzene modes and another family of 12 vibrational transitions arising from the e$_{2g}$ modes. Of the former set, there are two with appreciable IR intensity in the region 1480–1500 cm^{-1} in both the aryloxide and arylamide complexes. The observed IR spectra in the region 1570–1590 cm^{-1} correspond to transitions in the second family, as shown in Table 9. In the arylamide complexes the solution bands at 1572 and 1588 cm^{-1} correspond to the calculated transitions at 1579 and 1597 cm^{-1}. In the aryloxide dimer there are calculated bands at 1574 and 1596 cm^{-1} that agree well with experimentally observed bands at 1572 and 1588 cm^{-1}. In each case the lower energy band in the calculations corresponds to the vibrations of the bridging π-arene ligands. Thus the calculation of vibrational frequencies reveals the origin of the observed IR spectral behavior of both La$_2$(OAr)$_6$ and La$_2$(NHAr)$_6$, with the higher energy ν(C=C) stretch due to terminal ligands and the lower energy stretch associated with the bridging ligands. The shift to lower energy is due to electron donation to the La center upon coordination.

The effect of π-bonding on the bridging ligands can also be seen from the results of calculations carried out on the analogous O-bridged dimer (**II**) where there are no π-bonding interactions involving the metals. While this particular species has not been isolated, the analogous ammonia adduct La$_2$(μ-O-2,6-^{i}Pr$_2$C$_6$H$_3$)$_2$(O-2,6-^{i}Pr$_2$C$_6$H$_3$)$_4$(NH$_3$)$_2$ has been reported.[27] In the case of the theoretical O-bridged dimer **II**, the calculated IR frequencies for the bridging (1591 cm^{-1}) and terminal (1595, 1598 cm^{-1}) aryloxide ligands are much more similar than in the π-bridging case in Table 9, thus giving rise to a single strong band, as observed in the IR spectrum of La$_2$(μ-O-2,6-^{i}Pr$_2$C$_6$H$_3$)$_2$(O-2,6-^{i}Pr$_2$C$_6$H$_3$)$_4$(NH$_3$)$_2$ (1583 cm^{-1}).

Concluding Remarks

The structural similarities between La$_2$(OAr)$_6$ and La$_2$(NHAr)$_6$ complexes afford the opportunity to compare the solution chemical reactivity and nature of metal–ligand bonding in an essentially isostructural series of 4f element compounds. Both compounds exist in the solid state as the rather unusual π-arene-bridged dimeric unit. In both cases, we find the application of vibrational spectroscopy to be a very powerful tool for evaluating the π-arene interaction through changes in the ν(C=C) stretch upon coordination of an arene ring to the metal center.

Based on the remarkable similarity in the solid-state structures, with average La–C distances = 3.069(4) and 3.062(10) Å for arylamido and aryloxido ligands, one might not anticipate much difference in solution behavior. In a similar fashion, the vibrational spectroscopy reveals a shift to lower energy in the diagnostic ν(C=C) stretch upon coordination of the arene ring to the metal center. Here again, the observed frequency is 1572 cm^{-1} for both systems, suggesting little difference in the nature of metal–arene bonding interaction.

The observed solution chemistry, however, is markedly different between the two systems. La$_2$(NHAr)$_6$ reveals a monomer–dimer equilibrium in solution and reversible Lewis base adduct formation with THF. In contrast, La$_2$(OAr)$_6$ does not reveal an accessible equilibrium (by ^{1}H NMR), and once the Lewis base adducts are formed with THF, the ligands are not readily removed. These differences imply subtle differences in the nature of the La–arene bond, brought about by differences in electronic structure between OAr and NHAr ligands.

Examples of η^6-coordination of a neutral arene ring to a lanthanide metal center are increasingly common and generally fall into three structural types: (i) zero-valent lanthanides stabilized by two neutral 1,3,5-tri-*tert*-butylbenzene groups **VI**;[46] (ii) trivalent lanthanide centers with highly electron-withdrawing substituents such as halogenoaluminate [AlX$_4$]$^-$ **VII**[47−59] or dodecafluorodiphenyl amido ligands **VIII** (Ln = Nd);[45] and (iii) dimeric trivalent lanthanide compounds containing intermolecular π-arene interactions **IX**[6,24,25,27] or monomeric species containing intramolecular π-arene interactions **X**,[33,60,61] although a number of other less common structural motifs have been reported. [62]

VI   **VII**   **VIII**

IX   **X**
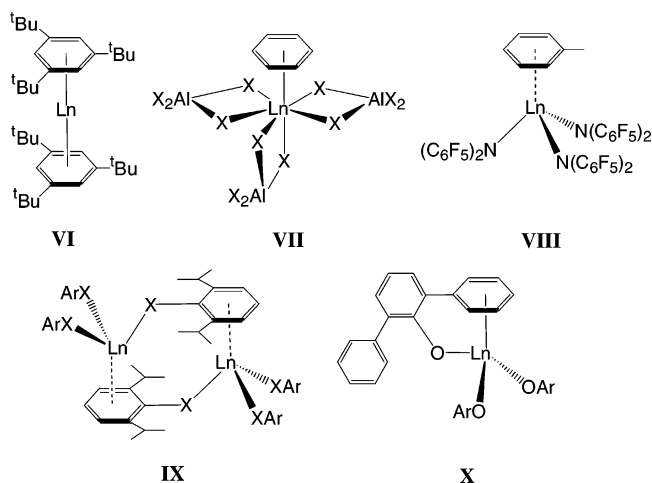
The nature of the lanthanide–arene chemical bond in the general class of zero-valent lanthanide complexes **VI** is very

(46) Brennan, J. G.; Cloke, F. G. N.; Sameh, A. A.; Zalkin, A. *Chem. Commun.* **1987**, 1668.

similar to the traditional description in d-block chemistry.[63−65] Computational studies indicate that the bonding interaction is best described as back-donation of a filled lanthanide 5d orbital into an unoccupied arene π^* acceptor orbital. The lanthanide−arene bonding in the other two classes of compounds exemplified by **VII−X** are more likely to originate from donation of filled π orbitals on the arene into unoccupied orbitals on the lanthanide metal center. The comparative study of OAr and NHAr ligands of structure type **IX** sheds additional light on this proposal. The calculations indicate that formation of η^6-arene interactions is energetically favored over monomeric LaX$_3$ (X= OPh or NHPh) and shows 6s/6p orbital contribution to bonding with the aryloxide π-arene interaction being stronger than the arylamide π-arene interaction. This order of stability is consistent with the observed chemical behavior and indicates that the aryloxide ligand has more electron density on the arene ring than the arylamide.

One simple means to rationalize which arene moiety will have the greatest electron density is to compare the acidity of the parent acids. It is well established that phenol is a stronger acid that aniline, due in part to the greater ability of the phenoxide anion to stabilize the negative charge on the arene ring compared to the corresponding anilide anion.[66] Thus the order OAr$^-$ > NHAr$^-$ suggests greater electron density on the OAr arene moiety than in the NHAr arene moiety, indicating that the aryloxide ligand would form the strongest metal−arene bonding interaction.

The metal−arene bonding is still admittedly weak, and electronic structure calculations were unable to identify a single molecular orbital interaction to account for the bonding. However, a Mulliken population analysis did reveal excess electron density in the otherwise virtual 5d La orbitals, consistent with the qualitative bonding picture. Of significance is that the calculations were able to predict two vibrational modes in the ν(C=C) stretching region of both the IR and Raman spectra and give close agreement between theory and experiment, identifying the origin of the two vibrational modes. The calculation of thermochemical data reproduce the relative strengths of La−π-arene interactions, with OAr > NHAr, and suggest an alternative description of the monomer−dimer equilibrium in **1**, to propose the involvement of the toluene

solvent to produce monomeric (η^6-C$_6$H$_5$Me)La(NHAr)$_3$. The calculations reproduce relative trends and give more insights into nature of bonding.

Experimental Section

General Considerations. All manipulations were carried out under an inert atmosphere of oxygen-free UHP grade argon using standard Schlenk techniques or under oxygen-free helium in a Vacuum Atmospheres glovebox. 2,6-Diisopropylaniline was purchased from Aldrich, dried over molecular sieves, and distilled over sodium prior to use. Pyridine was purchased from Aldrich and distilled over sodium benzophenone prior to use. La[N(SiMe$_3$)$_2$]$_3$[67] and [La(OAr)$_3$]$_2$ (**4**)[27] were prepared according to literature procedures. Hexane, toluene, and tetrahydrofuran were deoxygenated by passage through a column of supported copper redox catalyst (Cu-0226 S) and dried by passing through a second column of activated alumina.[68] C$_6$D$_6$, C$_7$D$_8$, d_8-THF, and d_5-pyridine were distilled over sodium benzophenone and degassed prior to use. ^{1}H and ^{13}C{^{1}H} NMR spectra were recorded on a Bruker AMX 300 spectrometer at ambient temperature unless otherwise noted. ^{1}H chemical shifts are given relative to residual C$_6$D$_5$H (δ = 7.15 ppm), C$_7$D$_7$H (δ = 2.09 ppm), C$_4$D$_7$HO (δ = 3.58 ppm), or C$_5$D$_4$HN (δ = 8.74 ppm). ^{13}C chemical shifts are given relative to C$_6$D$_6$ (δ = 128.39 ppm), C$_4$D$_8$O (δ = 67.57 ppm), or C$_5$D$_5$N (δ = 150.35 ppm). The ^{1}H NOESY spectrum was obtained on a Bruker DRX-500 spectrometer operating at 500.13 MHz in C$_7$D$_8$ at 318 K; t_1 was incremented in 512 steps, and the data were zero-filled to 1024 words before Fourier transformation. A total of 32 scans were recorded for each increment with t_{mix} = 250 ms with a relaxation time of 800 ms. Simulations of the variable-temperature ^{1}H NMR spectra in order to extract exchange constants were performed using DNMR71. Infrared spectra were recorded on a Nicolet Avatar 360 FT-IR spectrometer as Nujol mulls between KBr plates or as benzene solutions in a solution IR cell. Raman spectra were collected with a Nicolet Model 960 FT-Raman spectrometer attached to a Nicolet Model 560 Magna-IR with an extended XT-KBr beam splitter and 180° sampling geometry. The excitation source consisted of 0.24 W of 1064 nm light from a CW Nd:VO$_4$ laser. The interferogram was detected with an InGaAs detector operated at room temperature. An average of 128 and 1500 scans at 4 cm^{-1} resolution were taken for the solid compounds. Elemental analyses were performed by the Micro-Mass Facility at the University of California, Berkeley.

La$_2$(NH-2,6-^{i}Pr$_2$C$_6$H$_3$)$_6$ (1). 2,6-Diisopropylaniline (2.57 g, 14.5 mmol) in 10 mL of toluene was added to a pale yellow toluene solution (75 mL) of La[N(SiMe$_3$)$_2$]$_3$ (3.00 g, 4.84 mmol). This caused the formation of a bright yellow slurry. The reaction mixture was stirred at room temperature for 15 min and then heated to reflux for 15 min, during which time a golden yellow solution formed. Upon cooling, a bright yellow solid precipitated. The solvent was then removed under vacuum and the precipitate washed with hexane to remove HN(SiMe$_3$)$_2$. The resulting solid was collected by filtration and pumped to dryness (2.63 g, 80% yield). X-ray quality crystals were grown by evaporation of saturated toluene solutions of **1**. ^{1}H NMR (C$_6$D$_6$): δ 7.19 (d, $^3J_{H-H}$ = 7.2 Hz, 4H, *m*-H), 7.09 (d, $^3J_{H-H}$ = 7.2 Hz, 8H, *m*-H), 6.82 (t, $^3J_{H-H}$ = 7.2 Hz, 4H, *p*-H), 6.68 (t, $^3J_{H-H}$ = 7.2 Hz, 2H, *p*-H), 5.37 (s, 2H, N*H*), 5.12 (s, 4H, N*H*), 3.05 (sept, $^3J_{H-H}$ = 6.6 Hz, 8H, C*H*Me$_2$), 2.72 (sept, $^3J_{H-H}$ = 6.6 Hz, 4H, C*H*Me$_2$), 1.32 (d, $^3J_{H-H}$ = 6.6 Hz, 48H, CH*Me$_2$*), 1.24 (d, $^3J_{H-H}$ = 6.6 Hz, 24H, CH*Me$_2$*). ^{13}C{^{1}H} NMR (C$_6$D$_6$): δ 157.90, 152.82, 137.22, 133.12, 126.03, 123.57, 116.94, 111.95, 31.76 (*C*HMe$_2$), 24.00 (*C*HMe$_2$), 22.27 (CH*Me$_2$*), 15.92 (CH*Me$_2$*). IR (Nujol, cm^{-1}): 1587 (m), 1575 (m), 1324 (s), 1251 (m), 1168 (m), 1149 (m), 1104 (m), 1055 (m), 1037 (m), 882 (w), 840 (s), 796 (s), 767 (s), 738 (s). Anal. Calcd for C$_{72}$H$_{108}$La$_2$N$_6$: C, 64.75; H, 8.15; N, 6.29. Found: C, 62.81; H, 8.50; N, 6.20.

(47) Cotton, F. A.; Schwotzer, W. *J. Am. Chem. Soc.* **1986**, *108*, 4657.
(48) Fan, B.; Shen, Q.; Lin, Y. *J. Organomet. Chem.* **1989**, *376*, 61.
(49) Fan, B.; Shen, Q.; Lin, Y. *J. Organomet. Chem.* **1989**, *377*, 51.
(50) Fan, B.; Shen, Q.; Lin, Y. *Youji Huaxue* **1989**, *9*, 414.
(51) Liang, H.; Shen, Q.; Jin, S.; Lin, Y. *Chem. Commun.* **1992**, 480.
(52) Liang, H.; Shen, Q.; Guan, J.; Lin, Y. *J. Organomet. Chem.* **1994**, *474*, 113.
(53) Biagini, P.; Lugli, G.; Millini, R. *Gazz. Chim. Ital.* **1994**, *124*, 217.
(54) Biagini, P.; Lugi, G.; Abis, L.; Millini, R. *New J. Chem.* **1995**, *19*, 713.
(55) Liu, Q.; Lin, Y.; Shen, Q. *Acta Crystallogr., Sect. C* **1997**, *53*, 1579.
(56) Liu, Q.; Shen, Q.; Lin, Y.; Zhang, Y. *Chinese J. Inorg. Chem.* **1998**, *14*, 194.
(57) Troyanov, S. I. *Koord. Khim.* **1998**, *24*, 381.
(58) Troyanov, S. I. *Koord. Khim.* **1998**, *24*, 373.
(59) Troyanov, S. I. *Koord. Khim.* **1998**, *24*, 632.
(60) Deacon, G. B.; Nickel, S.; MacKinnon, P.; Tiekink, E. R. T. *Aust. J. Chem.* **1990**, *43*, 1245.
(61) Deacon, G. B.; Feng, T.; Forsyth, C. M.; Gitlits, A.; Hockless, D. C. R.; Shen, Q.; Skelton, B. W.; White, A. H. *Dalton Trans.* **2000**, 961.
(62) For a comprehensive review of Ln−arene complexes, see: Bochkarev, M. N. *Chem. Rev.* **2002**, *102*, 2089.
(63) King, W. A.; Marks, T. J.; Anderson, D. A.; Duncalk, D. J.; Cloke, F. G. N. *J. Am. Chem. Soc.* **1992**, *114*, 9221.
(64) King, W. A.; Di Bella, S.; Lanza, G.; Khan, K.; Duncalf, D. J.; Cloke, F. G. N.; Fragala, I. L.; Marks, T. J. *J. Am. Chem. Soc.* **1996**, *118*, 627 and references therein.
(65) Di Bella, S.; Lanza, G.; Fragala, I. L.; Marks, T. J. *Organometallics* **1996**, *15*, 3985.
(66) March, J. *Advanced Organic Chemistry*; Wiley: New York, 1985.

(67) Evans, W. J.; Golden, R. E.; Ziller, J. W. *Inorg. Chem.* **1991**, *30*, 4963.
(68) Pangborn, A. B.; Giardello, M. A.; Grubbs, R. H.; Rosen, R. K.; Timmers, F. J. *Organometallics* **1996**, *15*, 1518.

La(NH-2,6-ⁱPr₂C₆H₃)₃(THF)₃ (2). 1 (300 mg, 0.220 mmol) was dissolved in 5 mL of THF, forming a pale yellow solution. Slow evaporation resulted in large colorless crystals of **2** (330 mg, 84% yield). ¹H NMR (d_8-THF): δ 6.85 (d, $^3J_{H-H}$ = 8.0 Hz, 6H, *m*-H), 6.54 (t, $^3J_{H-H}$ = 8.0 Hz, 3H, *p*-H), 4.10 (s, 3H, N*H*), 3.55 (br t, 12H, α-C*H₂*), 2.95 (sept, $^3J_{H-H}$ = 7.2 Hz, 6H, C*H*Me₂), 1.70 (br t, 12H, β-C*H₂*), 1.16 (d, $^3J_{H-H}$ = 7.2 Hz, 36H, CH*Me₂*). ¹³C{¹H} NMR (d_8-THF): δ 154.60, 132.93, 122.82, 114.18, 68.38 (α-THF), 30.56 (*C*HMe₂), 26.53 (β-THF), 23.99 (CH*Me₂*). IR (Nujol, cm⁻¹): 1588 (m), 1420 (s), 1330 (s), 1299 (m), 1255 (s), 1221 (m), 1151 (m), 1138 (m), 1111 (m), 1083 (m), 1018 (m), 881 (m), 865 (m), 838 (s), 737 (s), 684 (m). Anal. Calcd for C₄₈H₇₈LaN₃O₃: C, 65.21; H, 8.89; N, 4.75. Found: C, 65.19; H, 8.82; N, 4.80.

La(NH-2,6-ⁱPr₂C₆H₃)₃(py)₂ (3). Toluene (5 mL) was added to **1** (300 mg, 0.220 mmol), forming a pale yellow slurry. Pyridine was added (1/2 mL), causing a pale yellow solution to form. Cooling to −30 °C resulted in large colorless crystals of **3** (140 mg, 75% yield). ¹H NMR (d_5-pyridine): δ 8.74 (s, 4H, *o*-py-H), 7.59 (s, 2H, *p*-py-H), 7.22 (s, 4H, *m*-py-H), 7.14 (d, $^3J_{H-H}$ = 7.5 Hz, 6H, *m*-H), 6.73 (t, $^3J_{H-H}$ = 8.0 Hz, 3H, *p*-H), 5.18 (s, 3H, N*H*), 3.33 (sept, $^3J_{H-H}$ = 6.6 Hz, 6H, C*H*Me₂), 1.18 (d, $^3J_{H-H}$ = 6.6 Hz, 36H, CH*Me₂*). ¹³C{¹H} NMR (d_5-pyridine): δ 155.14, 136.14, 133.47, 124.49, 123.32, 114.08, 30.19 (*C*HMe₂), 24.13 (CH*Me₂*) (one pyridine peak obscured by solvent resonance). IR (Nujol, cm⁻¹): 1623 (w), 1594 (s), 1588 (s), 1568 (sh), 1418 (s), 1331 (w), 1256 (s), 1215 (w), 1170 (w), 1150 (w), 1113 (w), 1055 (m), 1000 (m), 882 (w), 840 (m), 746 (m), 700 (m), 682 (m), 620 (m). Anal. Calcd for C₄₆H₆₄LaN₅: C, 66.89; H, 7.81; N, 8.48. Found: C, 65.86; H, 7.90; N, 8.34.

Crystallographic Studies. Crystals of **1**, **2**, and **3** were mounted on glass fibers using a spot of silicone grease. Due to air sensitivity, the crystals were mounted from a pool of mineral oil under argon gas flow. The crystals were placed on a Bruker P4/CCD diffractometer and cooled to 203 K using a Bruker LT-2 temperature device. The instrument was equipped with a sealed, graphite monochromatized Mo Kα X-ray source (λ = 0.71073 Å). A hemisphere of data was collected using φ scans, with 30 s frame exposures and 0.3° frame widths. Data collection and initial indexing and cell refinement were handled using SMART⁶⁹ software. Frame integration, including Lorentz-polarization corrections, and final cell parameter calculations were carried out using SAINT⁷⁰ software. The data were corrected for absorption using the SADABS⁷¹ program. Decay of reflection intensity was monitored via analysis of redundant frames. The structures were solved using Direct methods and difference Fourier techniques. For **2** and **3**, the amido hydrogen atom positions were located on the difference map and refined with isotropic temperature factor set to 0.08 Å². For **1** − **3**, all other hydrogen atom positions were idealized and rode on the atom they were attached to. The final refinement included anisotropic temperature factors on all non-hydrogen atoms. For **2**, the electron density of a disordered THF molecule was removed from the unit cell using PLATON/SQUEEZE.⁷² This resulted in two THF molecules per cell being removed (74 e⁻/cell and 326 Å³). For **3**, the structure was refined as a racemic twin, with the minor component batch-scale-factor converging to 0.423(8). Structure solution, refinement, graphics, and creation of publication materials were performed using SHELXTL NT.⁷³ Additional details of data collection and structure refinement are listed in Table 4.

Details of Theoretical Calculations. All calculations were carried out using the B3LYP functional⁷⁴ and employing relativistic effective core potentials (RECP) on the La atoms.⁷⁵,⁷⁶ All calculations used the "large core" RECP in which the 5s² 5p⁶ 6s² 5d¹ electrons were explicitly treated as "valence" electrons with the remaining electrons replaced by the RECP. The starting basis set for the -OAr and -NHAr ligands was the 6-31G basis. Additional calculations were carried out using the 6-31G* basis including d functions on all first-row atoms. The effects of diffuse functions on the heteroatoms were examined using the 6-31+G* basis, but these additional functions did not affect any calculated energy differences significantly. The calculations employed Gaussian 98⁷⁷ and Gaussian 03.⁷⁸ All structures were optimized in the 6-31G basis in B3LYP calculations. Vibrational frequencies were calculated at the resulting geometry for selected complexes discussed in the paper.

Supporting Information Available: Crystallographic data in CIF format for **1**−**3**, coordinates for the optimized model structures La₂(μ-OPh)₂(OPh)₄ and La₂(μ-NHPh)₂(NHPh)₄, and full details of the kinetic and thermodynamic analyses. This material is available free of charge via the Internet at http://pubs.acs.org.

JA0398262

(73) SHELXTL NT Version 5.10, Bruker Analytical X-ray Instruments, Madison, WI 53719, 1997.
(74) Becke, A. D. *J. Chem. Phys.* **1993**, *98*, 5648.
(75) Dolg, M.; Stoll, H.; Savin, A.; Preuss, H. *Theor. Chim. Acta* **1989**, *75*, 173.
(76) Dolg, M.; Stoll, H.; Preuss, H. J. *J. Chem. Phys.* **1989**, *90*, 1730.
(77) Frisch, M. J.; Trucks, G. W.; Schlegel, H. B.; Scuseria, G. E.; Robb, M. A.; Cheeseman, J. R.; Zakrzewski, V. G.; Montgomery, J. A.; Stratmann, R. E.; Burant, J. C.; Dapprich, S.; Millam, J. M.; Daniels, A. D.; Kudin, K. N.; Strain, M. C.; Farkas, O.; Tomasi, J.; Barone, V.; Cossi, M.; Cammi, R.; Mennucci, B.; Pomelli, C.; Adamo, C.; Clifford, S.; Ochterski, J.; Petersson, G. A.; Ayala, P. Y.; Cui, Q.; Morokuma, K.; Malick, D. K.; Rabuck, A. D.; Raghavachari, K.; Foresman, J. B.; Cioslowski, J.; Ortiz, J. V.; Stefanov, B. B.; Liu, G.; Liashenko, A.; Piskorz, P.; Komarami, I.; Gomperts, R.; Martin, R. L.; Fox, D. J.; Keith, T.; Al-Laham, M. A.; Peng, C. Y.; Nanayakkara, A.; Gonzalez, C.; Challacombe, M.; Gill, P. M. W.; Johnson, B. G.; Chen, W.; Wong, M. W.; Andres, J. L.; Head-Gordon, M.; Replogle, E. S.; Pople, J. A.; *Gaussian 98*, revision A.9; Gaussian, Inc.: Pittsburgh, PA, 1998.
(78) Frisch, M. J.; Trucks, G. W.; Schlegel, H. B.; Scuseria, G. E.; Robb, M. A.; Cheeseman, J. R.; Montgomery, J. A.; Vreven, T.; Kudin, K. N.; Burant, J. C.; Millam, J. M.; Iyengar, S. S.; Tomasi, J.; Barone, V.; Mennucci, B.; Cossi, M.; Scalmani, G.; Rega, N.; Petersson, G. A.; Nakatsuji, H.; Hada, M.; Ehara, M.; Toyota, K.; Fukuda, R.; Hasegawa, J.; Ishida, M.; Nakajima, T.; Honda, Y.; Kitao, O.; Nakai, H.; Klene, M.; Li, X.; Knox, J. E.; Hratchian, H. P.; Cross, J. B.; Adamo, C.; Jaramillo, J.; Gomperts, R.; Stratmann, R. E.; Yazyev, O.; Austin, A. J.; Cammi, R.; Pomelli, C.; Ochterski, J. W.; Ayala, P. Y.; Morokuma, K.; Voth, G. A.; Salvador, P.; Dannenberg, J. J.; Zakrzewski, V. G.; Dapprich, S.; Daniels, A. D.; Strain, M. C.; Farkas, O.; Malick, D. K.; Rabuck, A. D.; Raghavachari, K.; Foresman, J. B.; Ortiz, J. V.; Cui, Q.; Baboul, A. G.; Clifford, S.; Cioslowski, J.; Stefanov, B. B.; Liu, G.; Liashenko, A.; Piskorz, P.; Komaromi, I.; Martin, R. L.; Fox, D. J.; Keith, T.; Al-Laham, M. A.; Peng, C. Y.; Nanayakkara, A.; Challacombe, M.; Gill, P. M. W.; Johnson, B.; Chen, W.; Wong, M. W.; Gonzalez, C.; Pople, J. A.; *Gaussian 03*, revision B.2; Gaussian, Inc.: Pittsburgh, PA, 2003.
(79) Clark, D. L.; Gordon, J. C.; Huffman, J. C.; Vincent-Hollis, R. L.; Watkin, J. G.; Zwick, B. D. *Inorg. Chem.* **1994**, *33*, 5903.

(69) Sheldrick, G. M. SMART Version 4.210, Bruker Analytical X-ray Systems, Madison, WI 53719, 1996.
(70) Sheldrick, G. M. SAINT Version 5.050, Bruker Analytical X-ray Systems, Madison, WI 53719, 1998.
(71) Sheldrick, G. M. SADABS, Program for area detector adsorption correction, Institute for Inorganic Chemistry, University of Gottingen, Germany, first release, 1996.
(72) Spek, A. L. *Acta Crystallogr.* **1990**, *A46*, C34.